



Cite this: *Nat. Prod. Rep.*, 2014, **31**, 1202

# Zampanolide and dactylolide: cytotoxic tubulin-assembly agents and promising anticancer leads

Qiao-Hong Chen<sup>\*a</sup> and David G. I. Kingston<sup>\*b</sup>

Covering: through January 2014

Zampanolide is a marine natural macrolide and a recent addition to the family of microtubule-stabilizing cytotoxic agents. Zampanolide exhibits unique effects on tubulin assembly and is more potent than paclitaxel against several multi-drug resistant cancer cell lines. A high-resolution crystal structure of  $\alpha\beta$ -tubulin in complex with zampanolide explains how taxane-site microtubule-stabilizing agents promote microtubule assemble and stability. This review provides an overview of current developments of zampanolide and its related but less potent analogue dactylolide, covering their natural sources and isolation, structure and conformation, cytotoxic potential, structure–activity studies, mechanism of action, and syntheses.

Received 2nd March 2014

DOI: 10.1039/c4np00024b

www.rsc.org/npr

1. Introduction
2. Natural sources, isolation, and structure determination
- 2.1 Natural sources and isolation
- 2.2 Structure and conformation
- 2.3 The optical rotations of zampanolide and dactylolide
3. Biological activities and SAR
- 3.1 Cytotoxicity and MDR susceptibility
- 3.2 Structure–activity relationships (SAR)
4. Mechanism of action
- 4.1 Introduction
- 4.2 Binding site on tubulin
- 4.3 Bioactive conformation on tubulin
- 4.4 Mechanism of microtubule stabilization
5. Total synthesis of zampanolide and dactylolide
- 5.1 Introduction
- 5.2 Smith's syntheses of (+)-zampanolide and (+)-dactylolide
- 5.3 Hoye's total synthesis of (–)-dactylolide and (–)-zampanolide
- 5.4 Floreancig's total synthesis of (+)-dactylolide
- 5.5 Jennings' total synthesis of (–)-dactylolide
- 5.6 Keck's synthesis of (+)-dactylolide
- 5.7 McLeod's total synthesis of (–)-dactylolide
- 5.8 Porco's synthesis of the macrolactone core of (–)-zampanolide

- 5.9 Uenishi's synthesis of (–)-zampanolide and (–)-dactylolide
- 5.10 Lee's synthesis of (–)-dactylolide
- 5.11 Hong's total synthesis of (+)-dactylolide
- 5.12 Ghosh's synthesis of (–)-zampanolide<sup>16,24</sup>
- 5.13 Altmann's total synthesis of (–)-zampanolide<sup>17,82</sup>
- 5.14 Summary and evaluation
6. Other synthetic studies
- 6.1 Construction of *cis* 2,6-disubstituted THP rings
- 6.2 Preparation of *N*-acyl hemiaminal model systems
7. Conclusions

## 1. Introduction

The year 1979 marked a significant turning point in understanding the mechanism of action of anticancer agents, when Susan Horwitz published her pivotal paper indicating that paclitaxel (Taxol®) promoted the polymerization of tubulin to microtubules.<sup>1,2</sup> The discovery of this mechanism, an unprecedented mechanism of action for an anticancer drug at the time, was a crucial factor in paclitaxel's development as one of the most important drugs available for the treatment of breast and ovarian cancers.<sup>3,4</sup> The clinical success of paclitaxel in first-line treatment of cancer spurred the interest of the natural products community in the discovery of other microtubule stabilizing agents (MSAs) with a diversity of chemical structures and sources, and MSAs now represent one of the most important classes of cytotoxic agents. At this time the epothilone derivative ixabepilone<sup>5</sup> is the only MSA besides the taxanes paclitaxel, docetaxel, and cabazitaxel<sup>4</sup> that has entered clinical use. It is however very likely that other MSAs will enter clinical use in the

<sup>a</sup>Department of Chemistry, California State University, Fresno, 2555 E. San Ramon Avenue, M/S SB70, Fresno, CA 93740, USA. E-mail: qchen@csufresno.edu; Fax: +1 559 2784402; Tel: +1 559 2782394

<sup>b</sup>Department of Chemistry and Virginia Tech Center for Drug Discovery, M/C 0212, Virginia Tech, Blacksburg, VA 24061, USA. E-mail: dkingston@vt.edu; Fax: +1 540 2313255; Tel: +1 540 2316570



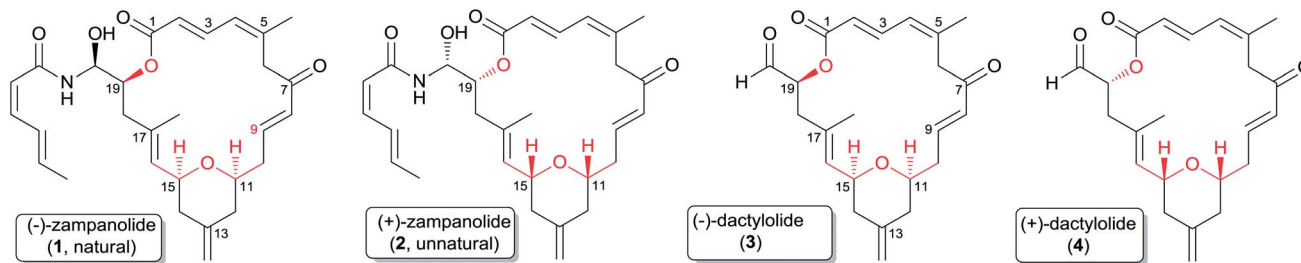


Fig. 1 Structures of zampanolide and dactylolide.

future, especially as novel MSAs with improved pharmacologic properties and potent activities against multi-drug resistant cancers continue to be discovered from nature,<sup>6</sup> and our understanding of the binding sites of these compounds continues to advance.

(–)-Zampanolide (1) (Fig. 1)<sup>7</sup> is a 20-membered polyketide first isolated from a marine sponge in 1996, and is a unique and recent addition to the class of MSAs.<sup>8</sup> It exhibits low nanomolar cytotoxicity against both drug sensitive and multi-drug resistant cancer cell lines, and induces microtubule bundle formation.<sup>8</sup> Its potent activity combined with its low number of chiral centres makes it an attractive compound for large-scale synthetic preparation for further study or clinical applications. As described in more detail below, the unique effects of zampanolide on tubulin assembly and its superior activity compared with that of paclitaxel against several multi-drug resistant cancer cell lines suggests that this natural macrocyclic compound could exhibit a unique spectrum of cytotoxic activities in a clinical setting and could be a valuable addition to existing anticancer drugs.

The related compound dactylolide was isolated from the marine sponge *Dactylospongia* sp. in 2001 by Riccio and co-workers,<sup>9</sup> and its core structure is the same (excluding stereochemistry) as the macrocyclic core of zampanolide. Its absolute

configuration has not been established, but as discussed in Section 2.3 it seems likely on biogenetic grounds that it is the same as that of (–)-zampanolide, which would make natural dactylolide the (–) isomer 3 in spite of its low (+) rotation (Fig. 1).

This review summarizes current knowledge about zampanolide and its structural relative dactylolide, covering their sources and isolation, structures, anticancer potential, mechanism of action, and syntheses.

## 2. Natural sources, isolation, and structure determination

### 2.1 Natural sources and isolation

(+)-Zampanolide (1) was first isolated in 1996 in 0.001% yield by Tanaka and Higa from 480 g of the marine sponge *Fasciospongia rimasa* collected off Cape Zampa on Okinawa.<sup>7</sup> It was isolated by repeated chromatography of the acetone extract of the sponge over silica gel and by ODS HPLC. It was re-isolated thirteen years later by Northcote and Miller and co-workers in an even lower 0.0005% yield from 341 g of the marine sponge *Cacospongia mycofijiensis* collected from an underwater cave off the Tongan coast.<sup>8</sup> Zampanolide was obtained from the 80% acetone–H<sub>2</sub>O fraction of the methanolic extract of the frozen sponge by



Qiao-Hong Chen received her Ph.D. degree from Sichuan University, China. Appointed as a Lecturer in 2001, she was promoted to the position of Full Professor in 2003 at Sichuan University. She was a Post-doctoral Fellow for three years at the University of Alberta in Canada and a Senior Research Fellow for six years at Virginia Tech in the USA. She started her current position as an Assistant

Professor of Chemistry at California State University, Fresno, in 2012. With her research interests focused on natural products-based anticancer agents, she is working to engineer drug-like analogs of zampanolide, curcumin, and genistein.



David Kingston received his Ph.D. degree from Cambridge University in 1964. He is currently a University Distinguished Professor of Chemistry and Director of the Virginia Tech Center for Drug Discovery. He has worked extensively on the chemistry and microtubule binding of paclitaxel and the epothilones, and he has carried out drug discovery work in Madagascar. He is a recipient of

the ACS Ernest Guenther Award in the Chemistry of Natural Products, and is a member of the NIH National Advisory Council for Complementary and Alternative Medicine. He also serves as one of several lay pastors in his local church, the Blacksburg Christian Fellowship.



sequential chromatography over a silica gel column and by HPLC.

Dactylolide was isolated in 2001 by Riccio from 353 g of a marine sponge of the genus *Dactylospongia* collected off the coast of Vanuatu.<sup>9</sup> It was obtained from the CCl<sub>4</sub> fraction of the methanolic extract through purification by medium pressure liquid chromatography over silica gel and by C-18 reversed-phase HPLC. Smith and co-workers found that thermolysis of synthetic (+)-zampanolide (**2**) in benzene provided (+)-dactylolide (**4**),<sup>10</sup> confirming the stereochemical relationship between (+)-zampanolide and (+)-dactylolide, and raising the possibility that dactylolide might be an artefact produced from decomposition of **2** during isolation. To test this hypothesis, Uenishi and co-workers exposed (–)-zampanolide and the sponge to the extraction conditions reported by Riccio and co-workers, and detected no trace of (–)-dactylolide (**3**) in either case.<sup>11</sup> They thus concluded that dactylolide is a naturally occurring entity instead of a degradation artefact of **1** or **2**.<sup>11</sup> However, this does not exclude the possibility that zampanolide could be a biosynthetic precursor of dactylolide.

## 2.2 Structure and conformation

The structure and partial stereochemistry of zampanolide were elucidated by Tanaka and Higa based on extensive interpretation of its 2D NMR spectra.<sup>7</sup> The relative configurations of the three chiral centres at C11, C15, and C19 were confirmed by observation of critical nOe correlations, but the relative configuration of C20 and the absolute configuration remained undetermined.<sup>7</sup> The complete stereochemistry was ultimately assigned by Smith and co-workers on the basis of the total synthesis of the unnatural antipode of zampanolide (**2**) in 2001.<sup>10,12</sup> The relative and absolute configurations of (+)-zampanolide were assigned as 11*R*, 15*R*, 19*R*, and 20*R* (Fig. 1). Zampanolide features a unique 20-membered macrolactone containing a *cis*-2,6-tetrahydropyran (THP), four olefinic bonds, and three chiral centres, and an uncommon *N*-acyl hemiaminal side chain with one chiral centre. Zampanolide is relatively hydrophobic in comparison with other macrolide MSAs and paclitaxel, as evidenced by its higher mobility on normal-phase TLC.

The planar structure of natural dactylolide was reported by Riccio and co-workers in 2001, also based on extensive spectroscopic analysis.<sup>9</sup>

The planar structures of zampanolide and dactylolide are very similar to each other, with the only difference being that the side chain in zampanolide is replaced by an aldehyde group in dactylolide. The chirality at C19 and the absolute configuration of natural dactylolide were not determined, but were assigned by Smith and co-workers on the basis of a total synthesis of **4** and the earlier conversion of **2** to **4**.<sup>10,13</sup> This work allowed assignment of the relative and absolute configurations of (+)-dactylolide as 11*R*, 15*R*, and 19*R*.<sup>10</sup> So far, no (+)-zampanolide has been isolated from nature.

Taylor and co-workers investigated the solution conformation behaviour of the macrolide core of (–)-zampanolide and (–)-dactylolide through a combination of high-field ROESY

NMR experiments and computational modeling.<sup>14</sup> Three interconverting conformational families, one of which bears a strong resemblance to zampanolide's tubulin-bound conformation, were found in solution for both molecules.<sup>14</sup> A rigid C15–C19 region and an *s-trans* northern diene are the common features shared by the three conformational families. The primary difference between the two major families [“hooked” (33%) and “flat” (35%)] is the orientation of the mostly inflexible northern fragment relative to the plane of the macrolide ring. The third conformational family (20%) features a twisted shape due to a 180° rotation around the C6–C7 bond. Although the western and diene segments are conformationally rigid, the macrolide has a flexible C6–C11 region, in part due to the ability of the C5–C6–C7–C8 torsion to adopt both 60° and 300° dihedral angles.<sup>14</sup>

## 2.3 The optical rotations of zampanolide and dactylolide

As shown in Table 1, there are significant deviations in optical rotations reported for the same compound from different sources. Keck<sup>15</sup> opined that the deviation may be caused by the enolization of a proton at C6, C10, or even the C5 methyl group. The enol content could vary with the use of different batches of solvent and/or different sources of the sample. For such highly conjugated enols, the measured optical rotation could be significantly different due to even small variations in enol content, and the large negative rotation of zampanolide is consistent with the large but variable negative rotations of the synthetic products with structure **1**. The configuration of naturally occurring zampanolide has thus been established as **1**.

The case of dactylolide is more complex, since the optical rotation value of the natural product is relatively small, and the rotations for natural and synthetic dactylolides are very different. Natural dactylolide has a rotation of +30, which is between the values for synthetic (+)-dactylolide, which range from +134 to +235, and synthetic (–)-dactylolide, which range from –128 to –258. Because the natural product has such a different rotation from both (+) and (–) synthetic enantiomers, the absolute configuration of the natural product cannot be considered to be established, and indeed the original paper on

Table 1 Optical rotations for zampanolide and dactylolide

Cmpd	Source	Optical rotation	Ref.
<b>1</b>	Sponge (Higa)	–101 ( <i>c</i> 0.12, CH <sub>2</sub> Cl <sub>2</sub> )	7
<b>1</b>	Sponge (Northcote)	–166 ( <i>c</i> 0.53, CH <sub>2</sub> Cl <sub>2</sub> )	8
<b>1</b>	Synthetic (Uenishi)	–98 ( <i>c</i> 0.07, CH <sub>2</sub> Cl <sub>2</sub> )	11
<b>1</b>	Synthetic (Ghosh)	–94 ( <i>c</i> 0.08, CH <sub>2</sub> Cl <sub>2</sub> )	16
<b>1</b>	Synthetic (Altmann)	–241 ( <i>c</i> 0.18, CHCl <sub>3</sub> )	17
<b>2</b>	Synthetic (Smith)	+102 ( <i>c</i> 0.09, CH <sub>2</sub> Cl <sub>2</sub> )	12
<b>3 or 4</b>	Sponge (Riccio)	+30 ( <i>c</i> 1.0, MeOH)	9
<b>3</b>	Synthetic (Hoye)	–128 ( <i>c</i> 0.39, MeOH)	18
<b>3</b>	Synthetic (Jennings)	–136 ( <i>c</i> 1.2, MeOH)	19
<b>3</b>	Synthetic (McLeod)	–169 ( <i>c</i> 0.42, MeOH)	20
<b>3</b>	Synthetic (Uenishi)	–168 ( <i>c</i> 0.45, MeOH)	11
<b>3</b>	Synthetic (Altmann)	–258 ( <i>c</i> 0.11, MeOH)	17
<b>4</b>	Synthetic (Smith)	+235 ( <i>c</i> 0.52, MeOH)	13
<b>4</b>	Synthetic (Floreancig)	+163 ( <i>c</i> 0.29, MeOH)	21
<b>4</b>	Synthetic (Keck)	+134 ( <i>c</i> 0.07, MeOH)	15



the isolation of dactylolide did not assign a configuration to the aldehyde at C19 or any absolute configuration to the other chiral centers.<sup>9</sup> Consequently, given the variation in optical rotations caused by varying amounts of enol form, and also given the fact that Hoyer and co-workers noted the propensity of the aldehyde of dactylolide to form a stable hemiacetal with methanol,<sup>18</sup> it is possible that naturally occurring dactylolide possesses the same absolute configuration as naturally occurring (–)-zampanolide and has a (–) rotation. Its small observed (+) rotation could be an artefact of enolization and/or hemiacetal formation. The strong probability that (–)-dactylolide is an intermediate in the biosynthesis of (–)-zampanolide (or *vice versa*) strengthens the assignment of natural dactylolide as **3**.

### 3. Biological activities and SAR

#### 3.1 Cytotoxicity and MDR susceptibility

(–)-Zampanolide was initially found to exhibit potent cytotoxicity ( $IC_{50}$  = 2–10 nM) against the P388, A549, HT29, and Mel28

cell lines.<sup>7,22</sup> Follow-up investigations demonstrated its low-nanomolar cytotoxicity against HL-60,<sup>8</sup> 1A9,<sup>8</sup> A2780,<sup>8,23</sup> OVCAR 8,<sup>24</sup> SKM-1,<sup>11</sup> and U937 (ref. 11) cell lines. More importantly, it also exhibits low nanomolar cytotoxicity against multi-drug resistant cancer cells that overexpress the P-gp multidrug resistance (MDR) pump, as shown in Table 2.<sup>8,24</sup> As noted by Diaz and his co-workers,<sup>23</sup> zampanolide is an interesting lead compound because of this diminished susceptibility. Such compounds may also have the potential for oral administration.<sup>25</sup> Covalent binding of a drug to its target can effectively inhibit the ability of P-gp to pump the drug out of the cell, and this has been demonstrated to be a method of avoiding P-gp mediated drug resistance in preclinical settings.<sup>6</sup> Since zampanolide binds covalently to tubulin, it has the potential to treat multi-drug resistant cancer.<sup>8</sup> Interestingly, (–)-dactylolide (**3**) also exhibits similar cytotoxicity towards both drug sensitive (A2780) and drug resistant cancer cells (A2780AD), even though it possesses much lower potency against these two cell lines than (–)-zampanolide (Table 2).

**Table 2**  $IC_{50}$  values (nM) for zampanolide and dactylolide against drug-sensitive and drug-resistant cancer cells

Cmpd	A2780	A2780AD	$R/S^a$	Ref.
<b>1</b>	$7.1 \pm 2.0$	$7.5 \pm 0.6$	1.1	8
<b>1</b>	$1.9 \pm 0.2$	$2.2 \pm 0.3$	1.2	23
<b>1</b>	$1.4 \pm 0.3$	$1.5 \pm 0.4$	1.1	23
<b>3</b>	$602 \pm 100$	$1236 \pm 180$	2.1	23
PTX	$2.8 \pm 1.4$	$415 \pm 48$	148	8
PTX	$0.46 \pm 0.1$	$1065 \pm 101$	2315	23
Cmpd	OVCAR 8	NCI/ADR-RES	$R/S^a$	Ref.
<b>1</b>	$20 \pm 0.6$	$25 \pm 7$	1.25	24
PTX	$7.5 \pm 2$	>5000	>667	24

<sup>a</sup> The relative resistance of the two cell lines obtained by dividing the  $IC_{50}$  of the resistant cell line by that of the parental cell line.

#### 3.2 Structure–activity relationships (SAR)

Only a small amount of structure–activity work has been reported on zampanolide (**1**). So far, all the available analogues (Fig. 2) for SAR investigation have come from synthetic by-products or from work from the Altmann laboratory. As shown in Table 3, its *N*-acyl hemiaminal side chain plays a dramatic role in the nanomolar  $IC_{50}$  values against the four cell lines tested.<sup>19</sup> Jennings' synthetic (–)-dactylolide (**3**) was 10- to 1000-fold less potent ( $GI_{50}$ ) than **1** against A549, HT29, and SK-Mel-28 cell lines. Interestingly, synthetic **3** is slightly more active than natural dactylolide against the SK-OV-3 cancer cell line.

The C20-epimer of **1** (**5**) and the bis-amide by-product (**6**)<sup>11,17,24</sup> are about one order of magnitude less potent than **1** in all the cell lines examined. Altmann's analogs **7**, **11**, and **12** showed comparable activity to that of **3**, suggesting that neither the aldehyde functionality nor the 13-methylene group are essential for the relatively weak antiproliferative activity of **3**.<sup>17</sup>

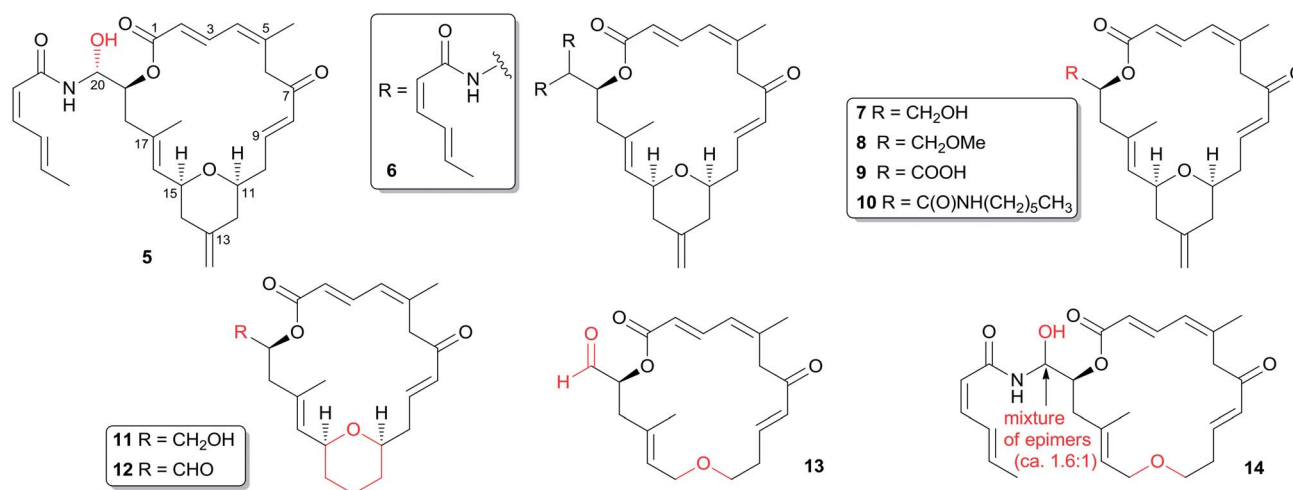


**Fig. 2** Zampanolide analogs.





Table 3 Antiproliferative activities of **1**, **3**, and **4**<sup>a</sup>

Cell line	<b>1</b>	<b>3</b>	<b>4</b>
A549 (ref. 17)	3.2 nM (ref. 17)	300 nM	
A549/ATCC	2–10 nM	4500 nM	
HT29	2–10 nM	263 nM	
SK-Mel-28	2–10 nM	5200 nM	
SK-OV-3		4700 nM	8300 <sup>b</sup> nM
P388	2–10 nM		
L1210			8300 <sup>c</sup> nM
SKM-1	1.1 nM (ref. 11)		
U937	2.9 nM (ref. 11)		
MCF-7 (ref. 17)	6.5 nM	250 nM	
PC-3 (ref. 17)	2.9 nM	750 nM	

<sup>a</sup> GI<sub>50</sub> values: data from ref. 19 unless otherwise stated. <sup>b</sup> IC<sub>50</sub> or GI<sub>50</sub> value. <sup>c</sup> GI<sub>40</sub> value.

Table 4 IC<sub>50</sub> values (nM) for zampanolide and its analogs against four cell lines<sup>a</sup>

Comp.	A549	MCF-7	HCT116	PC-3
<b>1</b>	3.2 ± 0.4	6.5 ± 0.7	7.2 ± 0.8	2.9 ± 0.4
<b>3</b>	301 ± 4.3	247 ± 2.6	210 ± 4.7	751 ± 69
<b>5</b>	53 ± 5.9	42 ± 9.3	88 ± 5.1	50 ± 11.7
<b>7</b>	127 ± 2.9	106 ± 3.6	155 ± 2.1	320 ± 26
<b>8</b>	1072 ± 103	1498 ± 83	1603 ± 122	1274 ± 117
<b>9</b>	9732 ± 260	7624 ± 303	12733 ± 379	9338 ± 242
<b>10</b>	973 ± 90	1138 ± 72	1204 ± 63	829 ± 27
<b>11</b>	189 ± 19.3	114 ± 10.2	74 ± 1.5	104 ± 4.1
<b>12</b>	149 ± 12.8	68 ± 5.6	249 ± 28	—
<b>13</b>	3921 ± 216	2894 ± 144	2653 ± 68	4021 ± 102
<b>14</b>	—	165 ± 13	309 ± 47	218 ± 7

<sup>a</sup> Data from ref. 17.

Conversion of the C20-hydroxyl group in **7** to the C20-methoxyl group in **8** leads to a 14-fold loss in antiproliferative potency. Carboxylic acid **9** is significantly less potent than the corresponding primary alcohol **7**. Interestingly, amide **10** is about 10-fold more potent than acid **9**, although the latter compound is several hundred-fold less potent than zampanolide. The encouraging activity of **10** suggests that fine-tuning of the substituent moiety on the amide nitrogen might be a way to develop improved analogs. The most intriguing analog from the Altmann laboratory is compound **14**, with submicromolar activity and a simple ether instead of the THP ring of the parent compound. Although the compound is 25 to 80-fold less potent than zampanolide, its activity is still very good in light of the removal of half the chiral centres and a rigidifying structural element. The corresponding (–)-dactylolide derivative (**13**) is about an order of magnitude less active than **14**. It is important to note that **14** is a *ca.* 1.6 : 1 mixture of diastereomers, suggesting that the IC<sub>50</sub> values for 18S-**14** could in fact be lower than observed (Table 4). These structure–cytotoxicity relationships are consistent with the results expected from the X-ray binding structure of zampanolide and β-tubulin, as discussed in Section 4.3.

## 4. Mechanism of action

### 4.1 Introduction

As noted above, zampanolide is a novel and potent MSA with properties similar to those of paclitaxel and docetaxel, stoichiometrically inducing tubulin assembly. It arrests cells in the G2/M phase of the cell cycle, induces microtubule bundles in interphase cells and spindle asters in dividing cells, and causes a dose-dependent shift of soluble tubulin to polymerized tubulin in cells and with purified tubulin.<sup>8,26</sup> It competes with paclitaxel for binding to microtubules,<sup>23</sup> but its mechanism of action is very different from paclitaxel's, as it involves covalent binding to β-tubulin, whereas paclitaxel binds non-covalently. The following sections describe its binding site and its mechanism of action in more detail.

### 4.2 Binding site on tubulin

There are three distinct binding sites for MSAs on microtubules: the taxane luminal site, the taxane pore site, and the peloruside site. The taxane luminal site is the classical taxane binding site that has been mapped to β-tubulin on the interior lumen of the microtubule.<sup>27</sup> Such a luminal location makes access to the binding site difficult in assembled microtubules. Kinetic data suggested that MSAs are able to access this site only after initially binding to a low-affinity site on the exterior of the microtubule.<sup>28</sup> The exterior site was later identified as the Thr<sup>220</sup> taxane pore binding site by Diaz and co-workers when they investigated cyclostreptin, the first MSA known to bind covalently to microtubules.<sup>29,30</sup> The third MSA binding site is entirely distinct from the taxane site and is targeted by the natural products laulimalide and peloruside A. Mass shift perturbation analysis in combination with data-directed computational docking were used to demonstrate that peloruside A and laulimalide bind to β-tubulin on the exterior surface of the microtubule.<sup>31,32</sup>

The first direct evidence for the binding site of zampanolide on tubulin was provided by Diaz and co-workers, who used mass spectrometry to determine the binding sites of both zampanolide and dactylolide on β-tubulin,<sup>23</sup> and provided a step-by-step protocol for this procedure.<sup>33</sup> Both zampanolide (**1**) and synthetic (–)-dactylolide (**3**) bind with a 1 : 1 stoichiometry, and compete with paclitaxel for binding to microtubules.<sup>23</sup> High resolution mass spectrometry showed that zampanolide binds to β-tubulin by irreversible alkylation of residues Asn<sup>228</sup> and His<sup>229</sup> at the taxane luminal site on the microtubule, with binding at His<sup>229</sup> yielding a significantly more abundant fragment ion than binding at Asn<sup>228</sup>. Zampanolide was able to bind to these amino acids in both dimeric tubulin and intact microtubules, indicating that the taxane luminal site is accessible in intact microtubules and also exists in tubulin dimers. In addition, since the binding to the luminal site occurs with a 1 : 1 stoichiometry, zampanolide does not bind at the pore site. Zampanolide strongly inhibited paclitaxel binding without interfering with peloruside A binding, and its specific binding to the taxane luminal site can impede or modify the taxane pore site. Thus hexaflutax (a fluorescent taxane probe that binds to



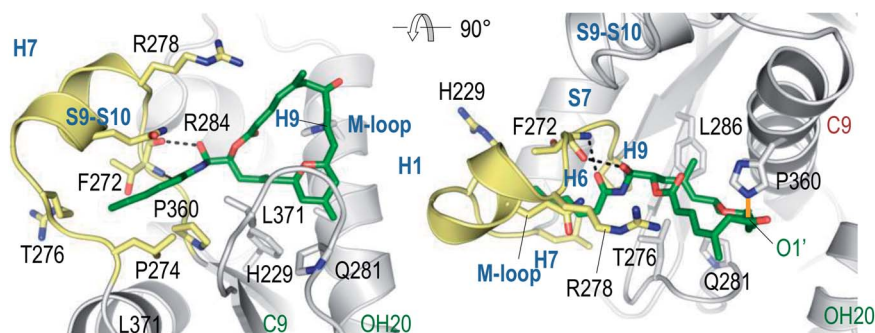


Fig. 3 Two views of the tubulin–zampanolide complex at 1.8 Å resolution. Adapted from *Science*, 2013, 339, 587–590 with permission.

the taxane pore site<sup>34</sup>) did not bind to tubulin in the presence of zampanolide even at stoichiometric concentrations with tubulin.<sup>23</sup> The apparent binding constants of both **1** and **3** increased with temperature, indicating possible covalent binding to microtubules,<sup>35,36</sup> similar to that of cyclostreptin.<sup>37</sup>

In an important publication Steinmetz *et al.* reported the structure of  $\alpha,\beta$ -tubulin complexed with the stathmin-like protein RB3, tubulin–tyrosine ligase, and zampanolide at 1.8 Å resolution (Fig. 3).<sup>38</sup> This structure clearly showed that zampanolide was deeply buried in the taxane luminal binding pocket formed by hydrophobic residues of helix H7,  $\beta$  strand S7, and the M-loop, and that its C9 atom was covalently bound to the NE2 atom of His<sup>229</sup> of  $\beta$ -tubulin, consistent with the major fragment ion in the mass spectrometric results described above.<sup>23</sup>

Kinetic binding studies of **1** and **3** using HPLC and fluorescence methods indicated that (–)-zampanolide reacted covalently with the taxane luminal site on both assembled microtubules and unassembled tubulin at a faster rate and more extensively than (–)-dactylolide.<sup>23</sup> (–)-Zampanolide has similar binding modes with both microtubules and unassembled tubulin, but (–)-dactylolide has three binding modes with microtubules and two binding modes with unassembled tubulin.<sup>23</sup>

### 4.3 Bioactive conformation on tubulin

The bioactive conformation of dactylolide bound to the tubulin  $\alpha,\beta$ -heterodimer and MTs was deduced by analysis of TR-NOESY crosspeaks. This was then used to build a putative zampanolide bioactive conformation.<sup>23</sup> This binding conformation was then confirmed by the crystal structure of the zampanolide tubulin complex noted above.<sup>38</sup> In this conformation, the 20OH group and the 1'O atom of zampanolide are hydrogen bonded to the main-chain carbonyl oxygen and the NH group of Thr<sup>276</sup>, respectively. The helical conformation of the M-loop is induced by the hydrophobic and polar contacts between the side chain of zampanolide and residues of the M-loop. This bound conformation closely resembles the major solution conformation found by Taylor *et al.*, albeit with a change to an *s-cis* orientation of the C7–C9 enone.<sup>14</sup>

This bioactive conformation is consistent with the cytotoxicities of zampanolide analogs summarized in Section 3.2. The

cytotoxicity for the C20-epimer of **1** is decreased due to the lack of hydrogen bonding between the 20OH group of zampanolide and the main-chain carbonyl oxygen of Thr<sup>276</sup>. The side chain of zampanolide is a major contributor to its potent cytotoxicity, due to its interaction with the M-loop, and the potent cytotoxicity of Altmann's simplified compound **14** can be explained by the fact that no critical interaction was observed between the THP ring of zampanolide and  $\beta$ -tubulin.

### 4.4 Mechanism of microtubule stabilization

As a covalent binding MSA, zampanolide induces microtubule polymerization through an allosteric effect in which the modified tubulin has a higher affinity towards polymerized microtubules than the unmodified fraction of tubulin.<sup>23</sup> The two types of contacts between tubulin subunits in the polymerization process are longitudinal contacts within protofilaments and lateral contacts between protofilaments.<sup>39</sup> It has been demonstrated that the M-loops of both  $\alpha$ - and  $\beta$ -tubulin play a central role in the lateral tubulin contacts in the absence of ligands.<sup>39,40</sup> The structure of the tubulin–zampanolide complex confirmed the existence of a short helix, consisting of residues Arg<sup>278</sup>–Tyr<sup>283</sup>, in the M-loop of  $\beta$ -tubulin.<sup>38</sup> Steinmetz *et al.* found that the MSA-stabilized helical M-loop conformation of  $\beta$ -tubulin agrees with the corresponding density of electron microscopy reconstructions of microtubules, and that Tyr<sup>283</sup> of the M-loop is inserted across protofilaments into a pocket shaped by the S2'–S2''  $\beta$ -hairpin and the H2–H3 loop of a neighbouring  $\beta$ -tubulin subunit. They also showed that the secondary structure elements of the taxane binding pocket were not significantly affected by the curved-to-straight tubulin conformational transition, and that the favourable positions of the M-loop residues Ser<sup>280</sup>, Gln<sup>282</sup>, Arg<sup>284</sup>, and Ala<sup>285</sup> provide additional contacts with the neighbouring  $\beta$ -tubulin. Based on these results, it was proposed that the binding of a MSA results in tubulin preorganization and subsequent reduction of the entropy loss associated with microtubule polymerization.<sup>38</sup>

Modeling of the helical conformation of the M-loop in the microtubule lattice, using the observed tubulin structure and cryogenic electron microscopy reconstructions of microtubules at  $\sim 8$  Å resolution, led Steinmetz *et al.* to propose that zampanolide and other taxane-site MSAs promote tubulin polymerization by binding to the taxane luminal site, converting the



disordered M-loop to a helix, and thus favouring polymerization. Microtubules that are formed spontaneously can also be stabilized by binding of the MSA to tubulin in the microtubule.

A recent computational docking study supported the paclitaxel site as the tubulin-binding site of zampanolide, and also indicated that His<sup>227</sup> is in a position to attack zampanolide and form a covalent bond.<sup>41</sup>

## 5. Total synthesis of zampanolide and dactylolide

### 5.1 Introduction

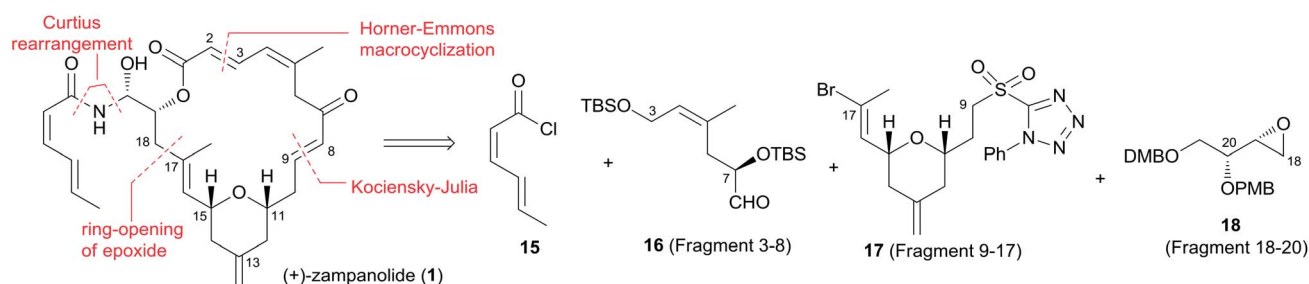
Twelve independent total syntheses of zampanolide, dactylolide and related macrolactone core have been achieved to date. Five synthetic approaches to zampanolide and dactylolide published prior to 2005 have been included in an earlier review,<sup>42</sup> and Sharif and O'Doherty<sup>43</sup> provided a condensation of and commentary on Smith's and Jennings' syntheses.

### 5.2 Smith's syntheses of (+)-zampanolide and (+)-dactylolide

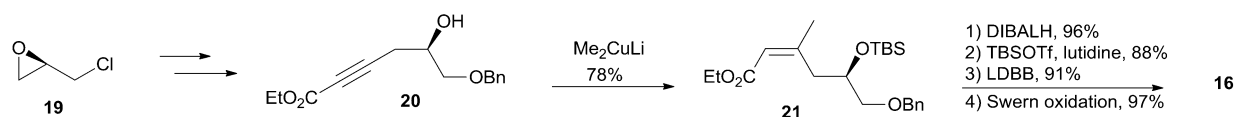
The first total synthesis of unnatural (+)-zampanolide (**2**) was achieved by the Smith group. Since neither the relative

configuration at C20 nor the absolute configuration of **1** had been defined at that time, they arbitrarily set **2** as their initial target.<sup>10</sup> Subsequently, the Smith group employed a similar synthetic strategy to synthesize (+)-dactylolide (**4**).<sup>10,13</sup>

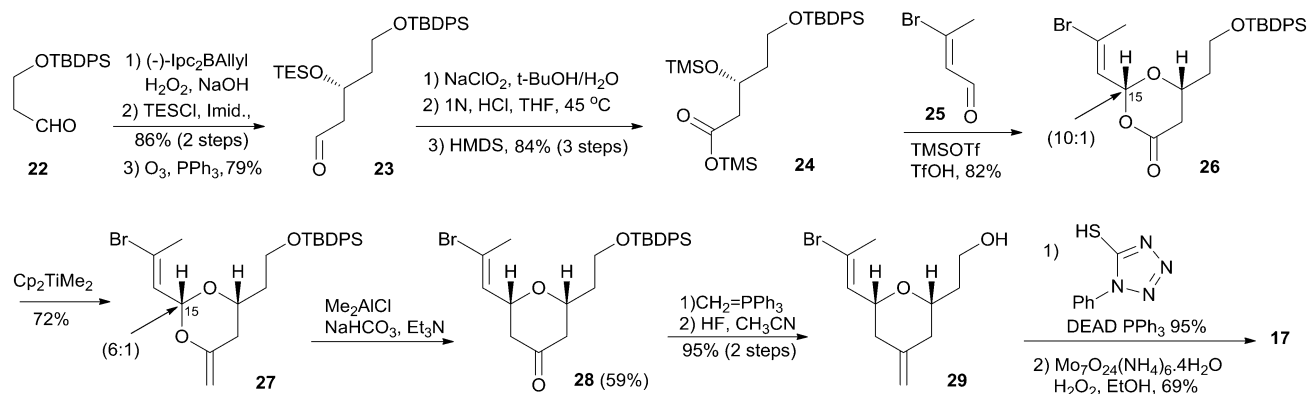
Smith's retrosynthetic analysis is outlined in Scheme 1.<sup>10,12,13</sup> A stereoselective Curtius rearrangement<sup>44</sup> was used to install the *N*-acyl hemiaminal side chain and Horner–Emmons macrocyclization<sup>45</sup> was employed to close the macrolactone ring at C2–C3. The macrocyclization precursor was constructed using nucleophilic epoxide ring-opening and Kocienski–Julia olefination as key reactions. The Petasis–Ferrier rearrangement was developed by Smith as a powerful and stereoselective approach to *cis*-2,6-disubstituted THP groups, and it was elegantly applied to the construction of the same unit in Smith's synthesis of zampanolide.<sup>46</sup> As shown in Scheme 2, fragment C3–C8 (**16**) was prepared from known alkynolate **20** (ref. 47) *via* a Michael-type carbometallation followed by four sequential reactions: reduction, protection, deprotection, and oxidation. The Smith synthesis of fragment C9–C20 is shown in Scheme 3. The aldehyde **23** was prepared *via* Brown asymmetric allylation of aldehyde **22**,<sup>48</sup> followed by silylation and oxidative cleavage of the terminal alkene. The aldehyde was readily converted to



Scheme 1 Smith's retrosynthetic analysis of (+)-zampanolide.



Scheme 2 Smith's synthesis of fragment C3–C8 of (+)-zampanolide.

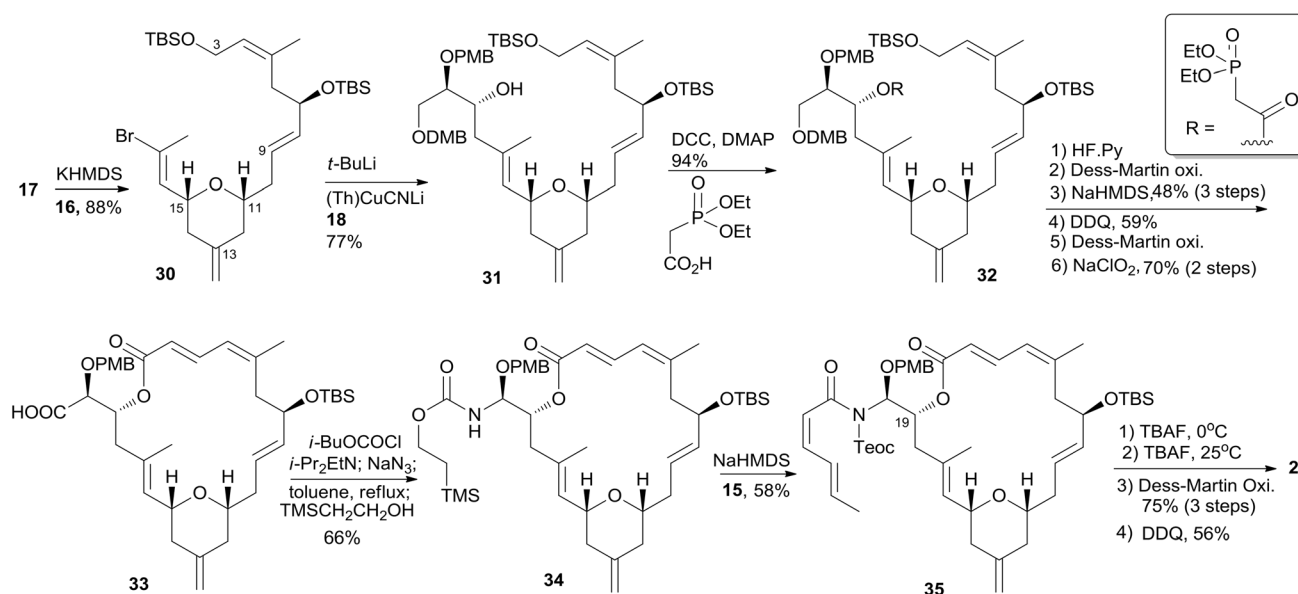


Scheme 3 Smith's synthesis of fragment C9–C17 of (+)-zampanolide.

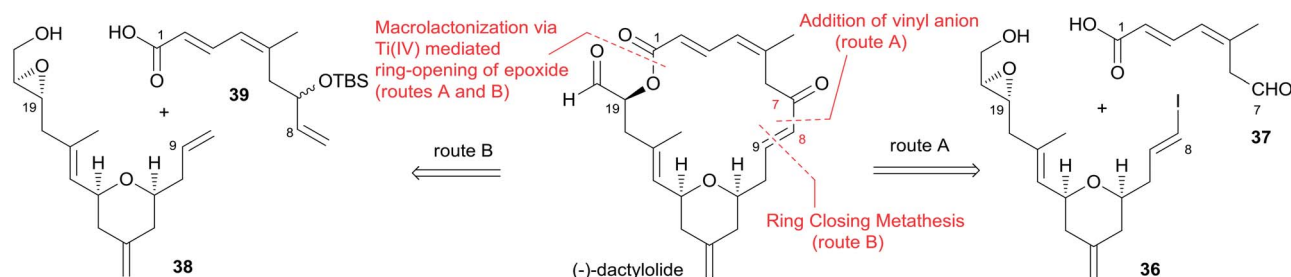


$\beta$ -hydroxy ester **24** in two steps, and this was condensed with aldehyde **25** mediated by TMSOTf to give a mixture of dioxanones **26** (10 : 1 at C-5). This cyclization was presumed to proceed *via* a transition state wherein the aldehyde side chain adopts a pseudoequatorial orientation. A mixture of the cyclic acetals **27** (6 : 1 at C-15) was achieved *via* the Petasis–Tebbe methylenation of **26**, which was subjected to the Petasis–Ferrier rearrangement with Me<sub>2</sub>AlCl to yield 2,6-*cis*-pyranone **28**. Wittig methylenation of ketone **28** followed by desilylation gave alkene **29**. Sulfone **17** was achieved by incorporation of the thiotetrazole *via* the Mitsunobu protocol and oxidation. Fragment C18–C21 (**18**) was prepared using (+)-diethyl tartrate as starting

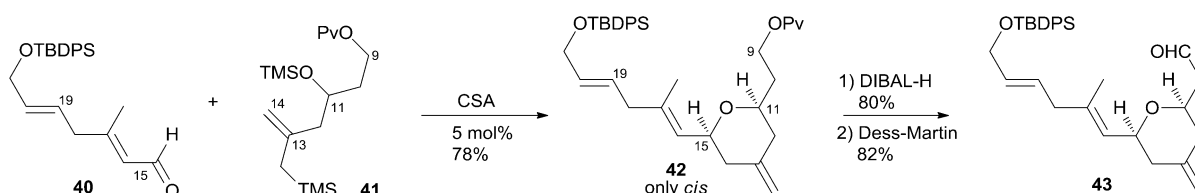
material through a seven-step sequence. As shown in Scheme 4, the *trans*-C8–C9 double bond in **30** was built by treating aldehyde **16** with sulfone **17** through the Kocienski–Julia olefination reaction. Fragment C3–C21 (**31**) was achieved by reaction of the mixed cyano–Gilman cuprate, derived from vinyl bromide **30** and lithium 2-thienylcyanocuprate, with epoxide **18**. Phosphonoacetate **32**, prepared by condensing diethylphosphonoacetic acid with **31**, was subjected to Horner–Emmons macrocyclization reaction and a following three-step sequence to provide carboxylic acid **33**. Carbamate **34** was prepared *via* Curtius rearrangement followed by treatment with trimethylsilyl ethanol. Transformation of carbamate **34** to (+)-zampanolide



Scheme 4 Smith's total synthesis of (+)-zampanolide.



Scheme 5 Hoye's retrosynthetic analysis of (–)-dactylolide.



Scheme 6 Hoye's synthesis of fragment C9–C20 of (–)-dactylolide.



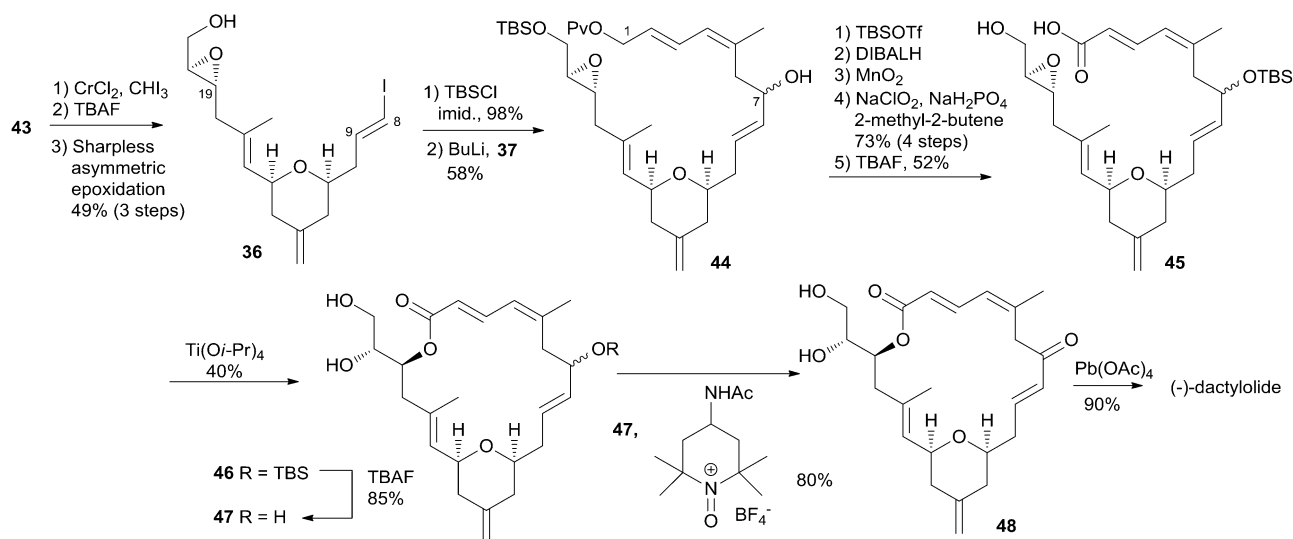


(2) was achieved by acylation with acid chloride **15** followed by a four-step, deprotection–oxidation sequence.

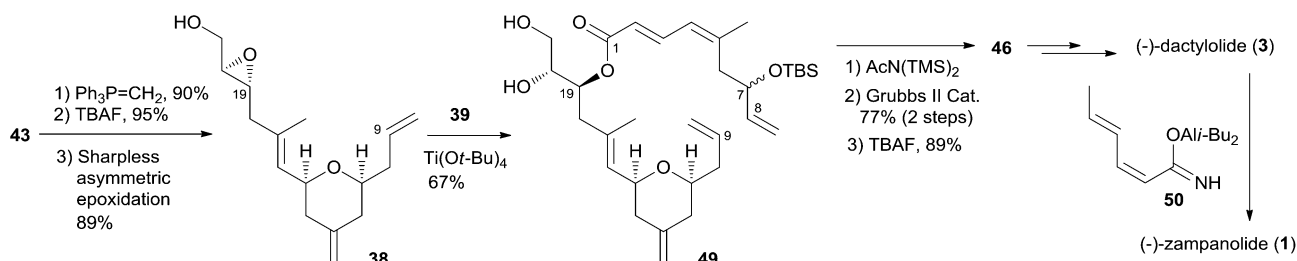
### 5.3 Hoye's total synthesis of (–)-dactylolide and (–)-zampanolide

Hoye and co-workers completed their syntheses of (–)-dactylolide (**3**)<sup>18</sup> using two strategies: (i) a novel Ti(IV)-mediated macrolactonization of an epoxy-acid (route A); and (ii) a complementary ring-closing metathesis (RCM) macrocyclization (route B) (Scheme 5). The fragment C9–C20 was constructed using Hosomi–Sakurai–Prins (HSP) cyclization as a key reaction (Scheme 6).<sup>49</sup> The 2,6-*cis*-THP **42**, which was readily

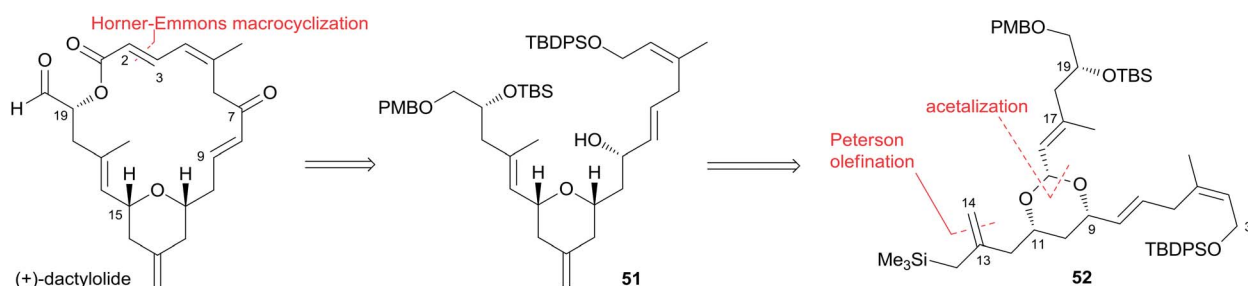
converted into aldehyde **43**, was exclusively generated by the HSP cyclization reaction<sup>49</sup> of enal **40** with allyl silane **41** (ref. 50) catalyzed by a protic acid. As shown in Scheme 7, aldehyde **43** was converted to epoxide **36** through a three-step sequence including Takai iodoalkenylation, desilylation, and Sharpless asymmetric epoxidation. Reaction of the alkenyllithium, prepared from epoxide **36** by protection followed by halogen–lithium exchange reaction, with aldehyde **37** generated fragment C1–C20 (**44**), which was converted into epoxy-carboxylic acid **45** in a five-step sequence. Macrolactone **46** was achieved by treating **45** with Ti(Oi-Pr)<sub>4</sub> under high dilution conditions. Sequential desilylation, oxidation of allylic alcohol, and oxidative cleavage of the C20–C21 diol generated **3**. Hoye's alternative



Scheme 7 Hoye's total synthesis of (–)-dactylolide.

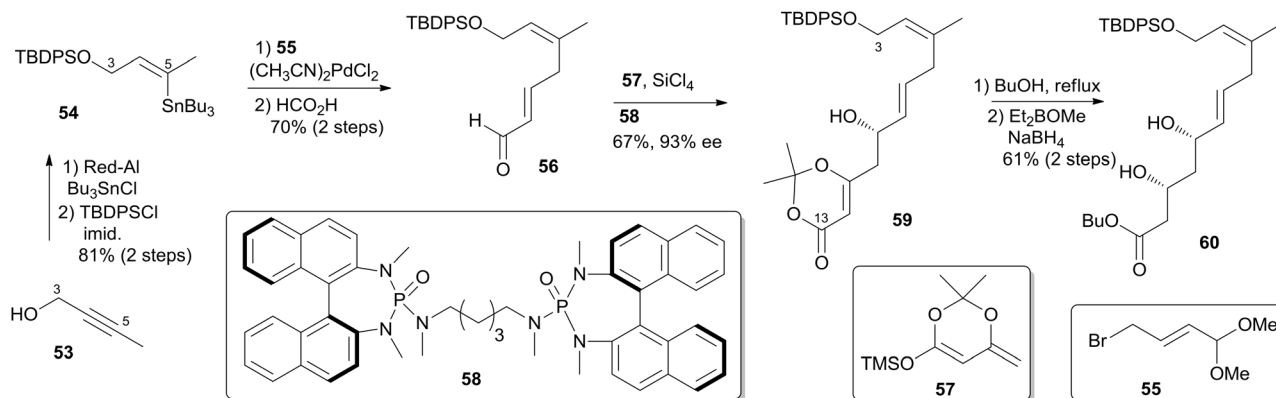


Scheme 8 Hoye's alternative total synthesis of (–)-dactylolide and (–)-zampanolide.

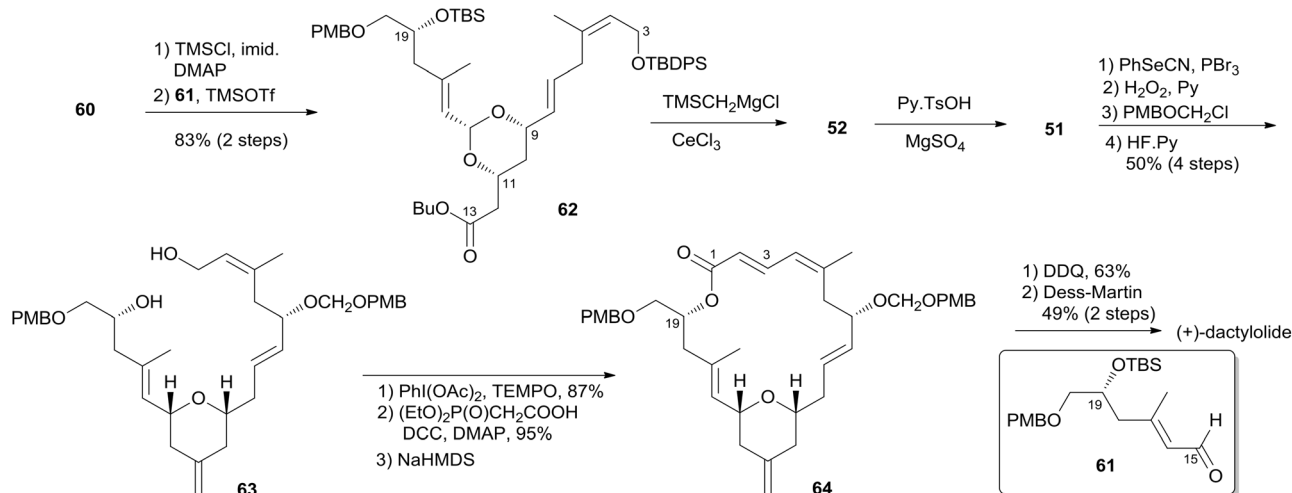


Scheme 9 Floreanci's retrosynthetic analysis of (+)-dactylolide.





Scheme 10 Floreancig's synthesis of fragment C3–C13 of (+)-dactylolide.



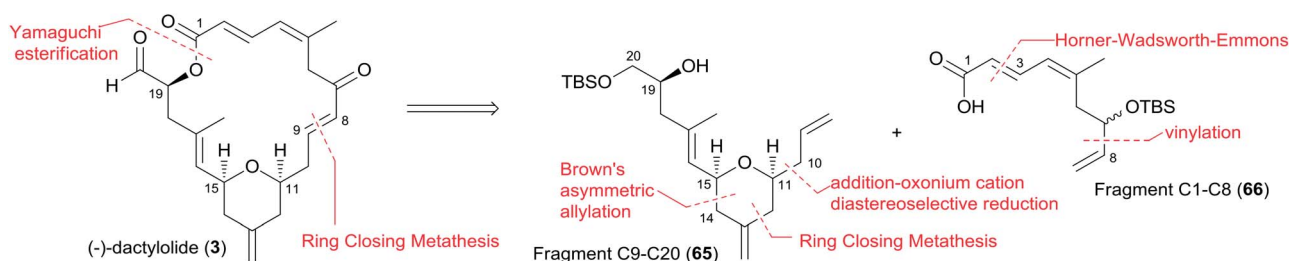
Scheme 11 Floreancig's total synthesis of (+)-dactylolide.

and more convergent synthesis of **3** as well as its subsequent conversion to **1** is shown in Scheme 8. Olefin **38**, prepared from aldehyde **43**, was coupled with trienoic acid **39** catalyzed by  $\text{Ti}(\text{Ot-Bu})_4$  to give diene precursor **49**. After protection of the vicinal diol *in situ* with excess bis-trimethylsilylacetamide, Grubbs RCM generated macrolactone **46** with an *E*-geometry of the C8–C9 alkene.

Compound **3** was converted to zampanolide *via* the aluminum aza-aldol addition of **50** in an unreported yield.

#### 5.4 Floreancig's total synthesis of (+)-dactylolide

Two key objectives to Floreancig's total synthesis of dactylolide were to maximize convergency and to minimize the number of carbon–carbon bond-forming reactions.<sup>21</sup> They postulated that the former objective could be achieved through the union of two advanced fragments by an acetal linkage. They envisioned asymmetric vinylogous Mukaiyama aldol reactions to be effective vehicles for achieving the latter objective. As shown in Floreancig's retrosynthetic analysis (Scheme 9), macrocyclization could be achieved by a Horner–Wadsworth–Emmons (HWE) reaction, the same strategy used in Smith's



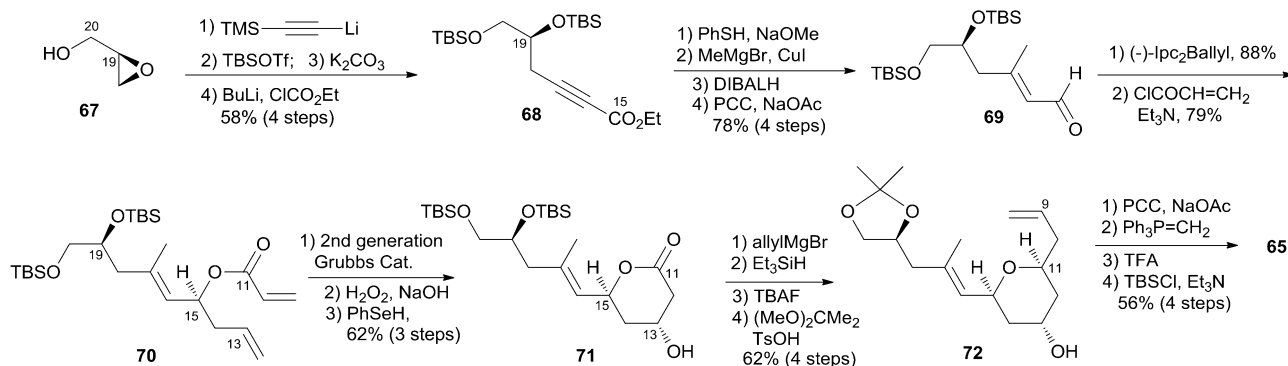
Scheme 12 Jennings' retrosynthetic analysis of (–)-dactylolide.

synthesis.<sup>10,12,13</sup> 2,6-*cis*-THP in fragment C3–C20 (**51**) could be constructed *via* the sequential cyclization starting from acetal **52**. Fragment C15–C20 (**61**) was prepared using the same procedure as described by Evans.<sup>51</sup> Fragment C3–C13 (**60**) was synthesized using the procedure as illustrated in Scheme 10. The (*Z*)-vinyl stannane **54** was prepared from hydroalumination of alkyne **53** followed by stannylation. Coupling of stannane **54** with bromide **55** followed by hydrolysis generated enal **56**. Ketal **59** was achieved in 93% ee through the asymmetric Mukaiyama aldol reaction of enal **56** with acetal **57** catalysed by Denmark's catalyst **58** and SiCl<sub>4</sub>. Fragment C3–C13 (**60**) was readily obtained by esterification of **59** followed by stereoselective reduction. Treatment of bis-TMS ether of **60** with aldehyde **61** mediated by TMSOTf provided the key acetal **62**. 2,6-*cis*-THP **51** was prepared by Peterson olefination of **62** with excess TMSMgCl and CeCl<sub>3</sub> followed by HSP cyclization catalysed by pyridinium triflate and MgSO<sub>4</sub>. The observed selectivity of kinetically facile 6-endo pathway over 8-endo pathway suggested that cyclization instead of ionization might be the product-determining step. Rearrangement of the C9 hydroxy group to C7 was achieved by a selenium variant of the Mislow–Evans rearrangement. Transformation from **51** to **63** was achieved in four steps. The corresponding phosphonoacetate,

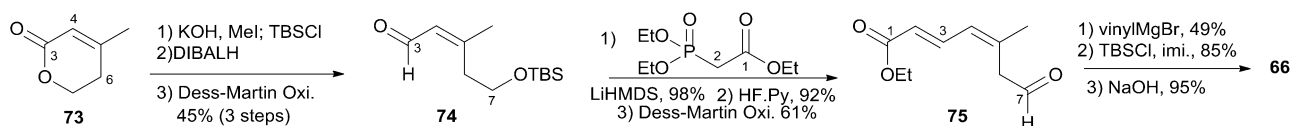
prepared by selective oxidation of allylic alcohol in **63** followed by esterification of C19 hydroxy group with phosphonoacetic acid, underwent intramolecular HWE reaction mediated by NaHMDS to generate macrolactone **64**. Finally, (+)-dactylolide was obtained through a deprotection–oxidation procedure (Scheme 11).

### 5.5 Jennings' total synthesis of (–)-dactylolide

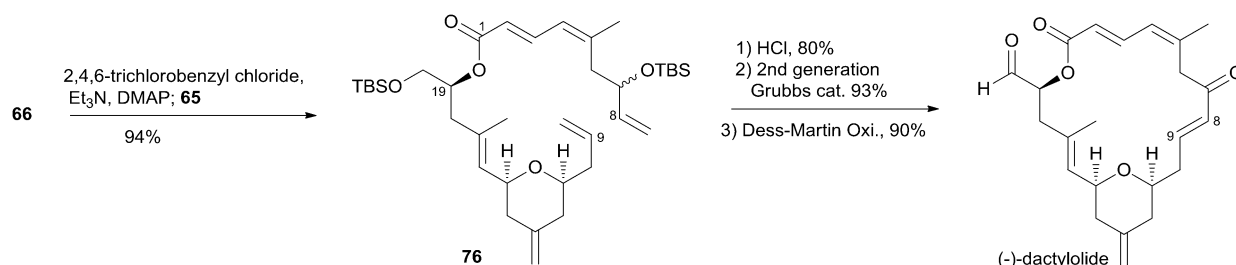
Jennings and co-workers constructed the macrolactone core structure by reaction of fragment C9–C20 (**65**) and fragment C1–C8 (**66**) by Yamaguchi esterification and RCM (Scheme 12).<sup>19,52</sup> Fragment C9–C20 (**65**) was constructed *via* diastereoselective axial reduction of an oxonium cation, RCM of a divinyl ester, and introduction of an asymmetric centre by Brown's asymmetric allylation. As delineated in Scheme 13, the  $\alpha,\beta$ -alkynyl ester **68**, prepared from glycidol **67** in four steps, was converted to enal **69** through a 4-step sequence: Michael addition of thiolate, copper-mediated 1,4-addition–elimination, reduction, and oxidation. Brown's asymmetric allylation of **69** followed by esterification furnished acrylate ester **70**. RCM of **70** followed by oxidation and reduction with PhSeH provided lactone **71**. 2,6-*cis*-THP **72** was prepared by the nucleophilic addition of ester **71**



Scheme 13 Jennings' synthesis of fragment C9–C20 of (–)-dactylolide.



Scheme 14 Jennings' synthesis of fragment C1–C8 of (–)-dactylolide.



Scheme 15 Jennings' total synthesis of (–)-dactylolide.

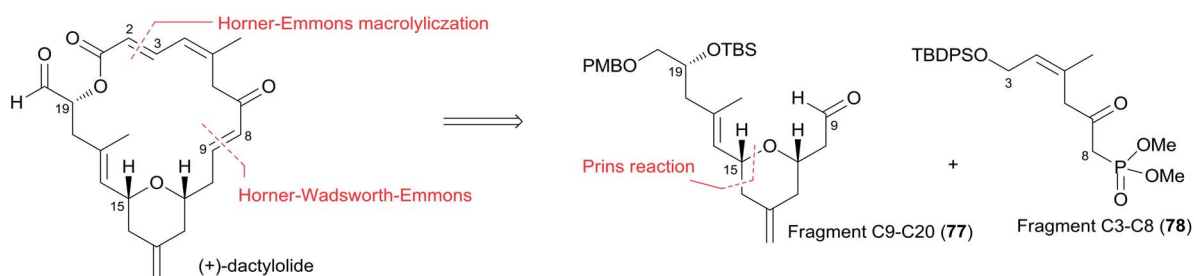


followed by diastereoselective reduction of oxonium cation. Fragment C9–C20 (**65**) was obtained in a four-step sequence: oxidation, methylenation, deprotection, and protection. Jennings' approach to fragment C1–C8 features a diastereoselective HWE, as shown in Scheme 14. The diene precursor **76** was made by Yamaguchi esterification of alcohol **65** with carboxylic acid **66** (Scheme 15). After removal of the protecting groups at C7 and C20, the corresponding diene was subjected to Grubbs' RCM to generate the desired macrolactone. Finally, (–)-dactylolide was obtained by oxidation with Dess–Martin reagent.

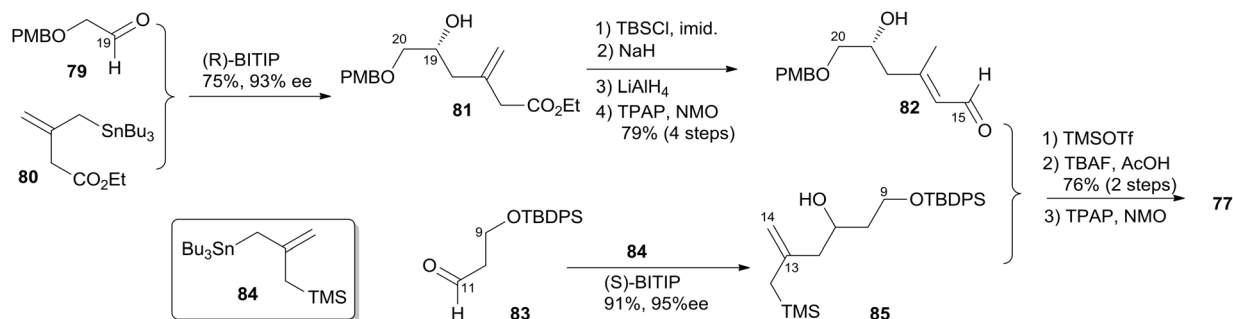
### 5.6 Keck's synthesis of (+)-dactylolide

Keck constructed the macrolactone core using HWE macrocyclization and the HSP reaction, featuring construction of two asymmetric centres *via* his catalytic asymmetric allylation

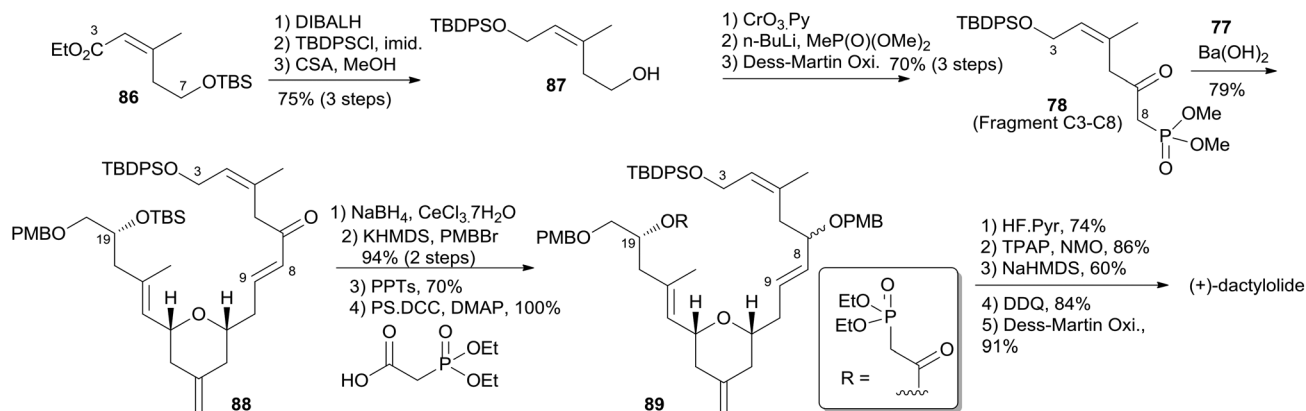
reaction and a diastereoselective pyran annulation (Scheme 16).<sup>53</sup> The preparation of fragment C9–C20 (**77**) is shown in Scheme 17. Asymmetric allylation of aldehyde **79** with allylstannane **80** catalyzed by BINOL titanium tetraisopropoxide (BITIP) gave (*R*)-homoallylic alcohol **81** in 93% ee. Isomerization to the (*E*)-unsaturated aldehyde **82** (32 : 1) was achieved by protection of the hydroxyl group, treatment with NaH, and a two-step reduction (Scheme 17). Keck and co-workers believed that the observed high stereoselectivity is a kinetic phenomenon associated with a preferred pathway for formation of the U shaped internally chelated enolate anion with sodium as counterion. Fragment C9–C14 (**85**) was prepared by asymmetric allylation of aldehyde **83** and allyl stannane **84** catalyzed by (*S*)-BITIP in 95% ee (Scheme 17). Fragment C9–C20 (**77**) was prepared by the HSP reaction between **82** and **85** followed by a



Scheme 16 Keck's retrosynthetic analysis of (+)-dactylolide.



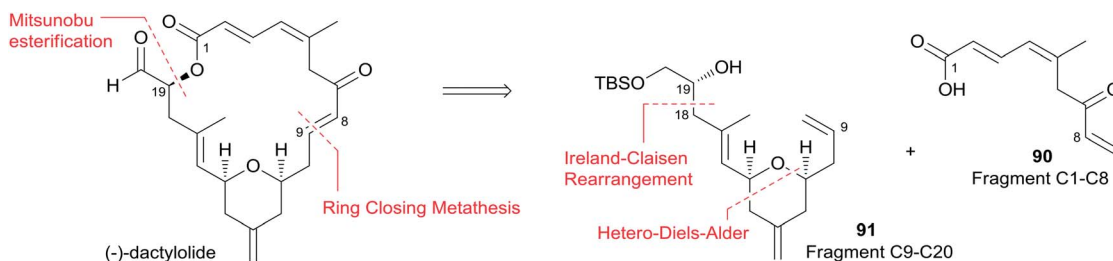
Scheme 17 Keck's synthesis of fragment C9–C20 of (+)-dactylolide.



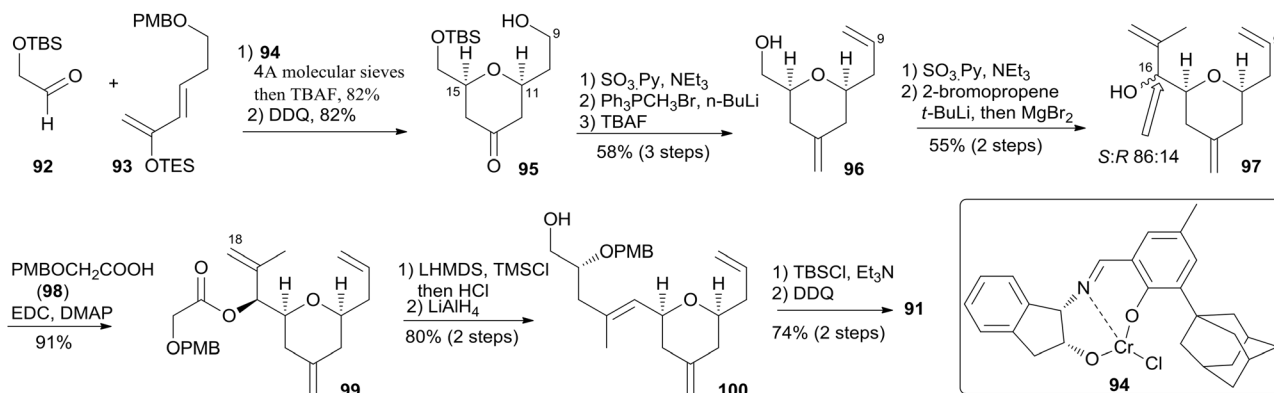
Scheme 18 Keck's total synthesis of (+)-dactylolide.



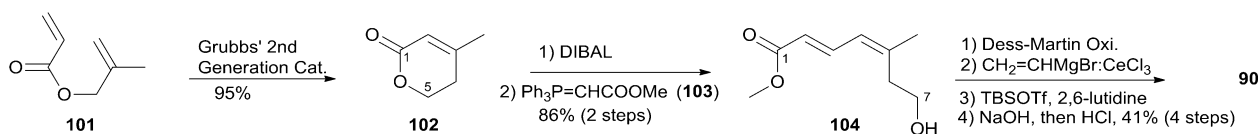




Scheme 19 McLeod's retrosynthetic analysis of (–)-dactylolide.



Scheme 20 McLeod's synthesis of fragment C9–C20 of (–)-dactylolide.



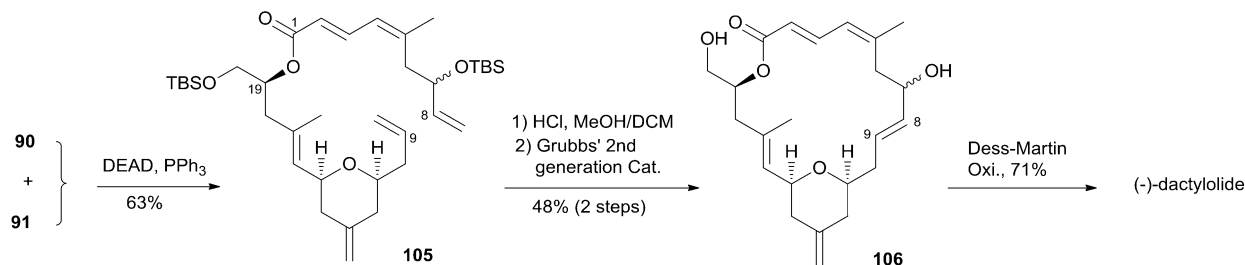
Scheme 21 McLeod's synthesis of fragment C1–C8 of (–)-dactylolide.

deprotection–oxidation procedure. The synthesis of fragment C3–C8 (**78**) began with intermediate **86** (ref. 54) (Scheme 18). Transformation of ester **86** to silyl ether **87** was carried out *via* a three-step sequence. The desired  $\beta$ -ketophosphonate **78** was achieved *via* another three-step sequence including oxidation, addition of the lithiate of methyl dimethyl phosphonate into this aldehyde, and oxidation of the resulting alcohol. HWE olefination of **77** with **78** under Peterson's conditions provided (*E*)-enone **88**. To avoid the possibility that the acidity of C6–H might cause C7 enolization, the ketone at C7 was converted to its PMB ether, which was selected by Keck because both PMB groups (at C7 and C20) could be deprotected and both alcohols oxidized in the same operation at the later stage. Next, phosphonoacetate **89** was prepared by selective deprotection and modified Keck–Boden macrolactonization.<sup>55</sup> A polymer-bound DCC (PS-DCC) rather than DCC itself was used to simplify the workup and purification due to the polarity of the phosphonate. Intramolecular HWE macrolactonization followed by PMB deprotection and double oxidation afforded **4** (Scheme 18).

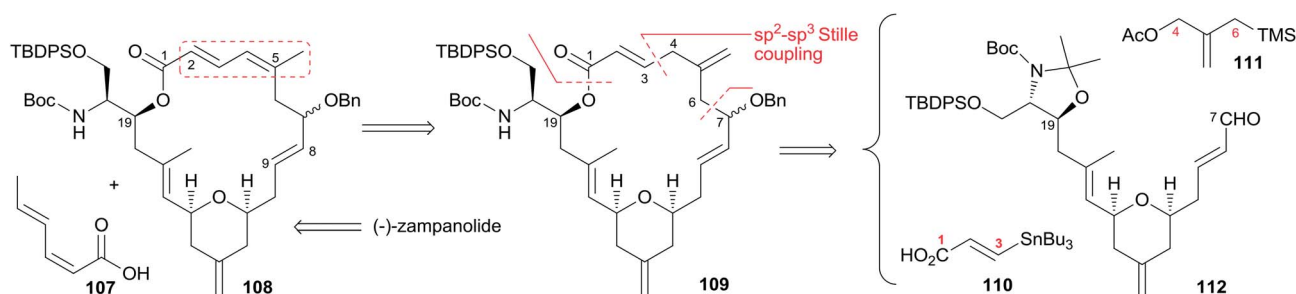
## 5.7 McLeod's total synthesis of (–)-dactylolide

McLeod reported an enantioselective synthesis of (–)-dactylolide, featuring the construction of the 2,6-*cis*-THP by catalytic asymmetric Jacobsen hetero-Diels–Alder reaction,<sup>56</sup> and the remote C19 chiral centre by a sequence of chelation-controlled Grignard addition and Ireland–Claisen rearrangement.<sup>20</sup> As shown in the retrosynthetic analysis (Scheme 19), the macro-lactone core was constructed by convergent coupling of fragment C1–C8 (**90**) and fragment C9–C20 (**91**) using a sequence of Mitsunobu esterification followed by Grubbs' RCM. The synthesis of **1** (Scheme 20) began with the linkage of aldehyde **92** and silyl enol ether **93** mediated by Jacobsen's chiral tridentate chromium(III) catalyst **94**. THP **95** can be synthesized on a multigram scale by careful workup followed by PMB removal. Diene **96** was synthesized through a three-step procedure including oxidation, Wittig methylenation, and silyl ether deprotection. Nucleophilic addition of isopropenyl Grignard to the aldehyde obtained by oxidation of **96** proceeded with chelation control to favour formation of **97** with the 16*S*-configuration. Alcohol **97** was then converted to ester **99** *via*





Scheme 22 McLeod's total synthesis of (-)-dactylolide.



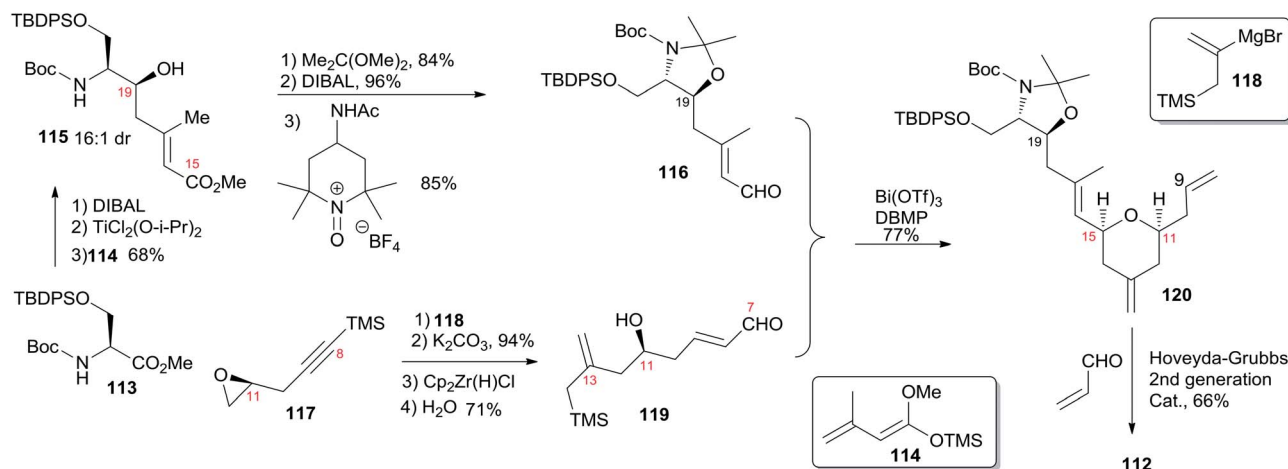
Scheme 23 Porco's retrosynthetic analysis of (-)-zampanolide.

esterification with PMB protected glycolic acid **98**. Direct reduction of a crude product of the polar carboxylic acid derived from the Ireland–Claisen [3,3] sigmatropic rearrangement of ester **99** gave alcohol **100** as a single diastereomer. Alcohol **100** was converted to alcohol **91** through a simple protection–deprotection procedure. Synthesis of trienoic acid **90** was completed (Scheme 21) in seven steps from acrylate ester **101** (ref. 57) with trisubstituted *Z*-alkene established *via* a six-membered lactone intermediate **102**. Direct Wittig reaction of the lactol derived from partial reduction of lactone **102** with ylide **103** afforded (2*E*, 4*Z*)-diene ester **104**. The aldehyde, derived from **104**, reacted with vinylcerium reagent, followed by a protection–hydrolysis procedure, to afford fragment C1–C8 (**90**). The final stage synthesis is shown in Scheme 22.

Mitsunobu esterification provided ester **105**. The diene precursor, derived from **105**, was subjected to a Grubbs RCM reaction to afford macrocyclic diols **106**, which were subjected to global oxidation to give (-)-dactylolide **3**.

### 5.8 Porco's synthesis of the macrolactone core of (-)-zampanolide

Porco's synthesis of the macrocyclic core of **1** was initiated by interest in the *N*-acyl hemiaminal side chain and its apparent stabilization through an intramolecular hydrogen bond network, and entailed preparation of an *N*-acyl hemiaminal model system.<sup>58,59</sup> The synthetic strategy is characterised by construction of fragment C15–C20 by a one-pot reduction/vinylogous aldol reaction, construction of the 2,6-*cis*-THP



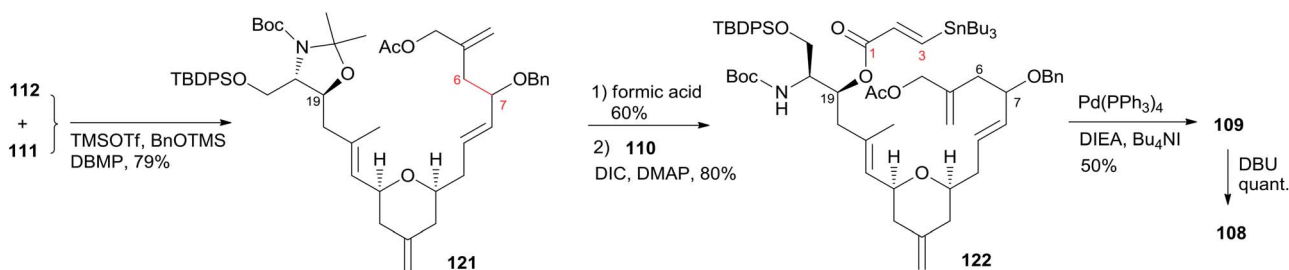
Scheme 24 Porco's synthesis of fragment C7–C20 of (-)-zampanolide.

through an intramolecular silyl-modified Sakurai (ISMS) reaction,<sup>60</sup> and closing the macrolactone ring *via* an  $sp^2$ – $sp^3$  Stille reaction. As outlined in Scheme 23, Porco's synthetic strategy for zampanolide is to install the *N*-acyl hemiaminal side chain from the protected amino alcohol-bearing macrolide **108** at a late stage using their previously reported oxidative decarboxylation–hydrolysis approach.<sup>59</sup> In order to install the potentially sensitive 1,3-dienoate portion of the macrolide at a late stage, these workers investigated a less conventional disconnection by targeting 1,4-dienoate **109** instead of 1,3-dienoate **108**. They expected that subsequent isomerization would occur under macrocyclic control and installation of the dienoate in a “masked” format would allow for unveiling after construction of the macrolide. Further disconnection of macrolide **109** afforded three precursors:  $\beta$ -stannylacrylic acid **110**, allylic acetate **111**, and the pyran containing the C7–C20 fragment **112**. The C3–C4 bond would be constructed *via* an intramolecular Stille reaction, representing a pioneer example of using an  $sp^2$ – $sp^3$  Stille macrocyclization in a complex synthesis. Synthesis of the C7–C20 fragment is shown in Scheme 24. The two-step process developed by Kiyooka<sup>61</sup> using DIBAL-H and  $TiCl_4(O-iPr)_2$  provided the desired vinylogous aldol product **115** (dr = 16 : 1) from methyl ester **113**. Vinylogous aldol substrate **115** was next advanced to the  $\alpha,\beta$ -unsaturated aldehyde **116** through a three-step sequence including protection of amino alcohol as the *N,O*-acetonide, reduction of the methyl ester, and subsequent oxidation with Bobbit's reagent.<sup>62</sup> The requisite allylsilane **119** for an intramolecular Sakurai cyclisation (IMSC)<sup>60</sup> reaction was obtained from Cu(I)-mediated addition of vinyl Grignard reagent **118** (ref. 63) to chiral epoxide **117** (ref. 64) (Scheme 24). The IMSC reaction of **116** and **119** mediated by  $Bi(OTf)_3$  in conjunction with 2,6-di-*tert*-butylpyridine as triflic acid

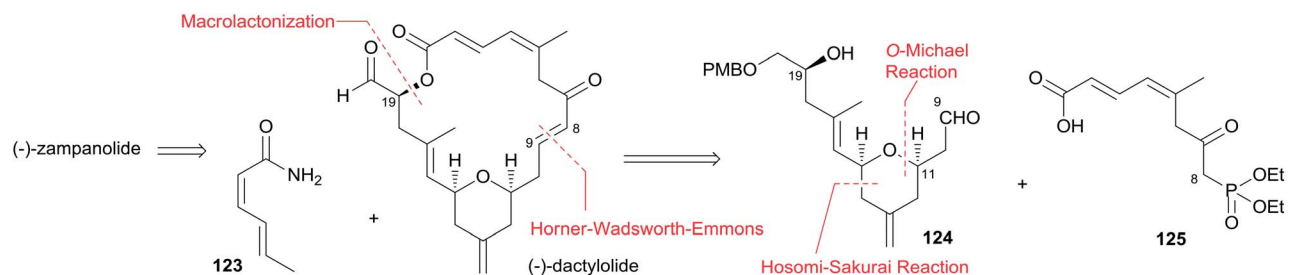
scavenger afforded pyran **120** as a single diastereomer. Elaboration of the terminal olefin by Grubbs–Hoveyda cross-metathesis provided  $\alpha,\beta$ -unsaturated aldehyde **112** (Scheme 24). Allylation of **112** with the Trost trimethylenemethane (TMM) reagent **111** (ref. 65) in the presence of  $BnOTMS$  afforded allylic acetate **121** (dr = 1 : 1) (Scheme 25). Removal of the acetonide protecting group followed by esterification with  $\beta$ -stannyl acrylate **110** (ref. 66) provided the macrocyclization precursor **122**. Macrocyclization of vinylstannane **122** was mediated by  $Pd(PPh_3)_4$ – $Bu_4NI$ – $DIEA$  to afford macrolactone **109**. Porco indicated that only 1,4-diene product was observed, likely due to the constraints of the macrolide on olefin isomerization. Subsequent isomerization by DBU resulted in formation of 1,3-diene **108** in quantitative yield as a 1 : 1 mixture of *E,Z*-isomers.

### 5.9 Uenishi's synthesis of (–)-zampanolide and (–)-dactylolide

Uenishi's retrosynthetic strategy is illustrated in Scheme 26.<sup>11</sup> The side chain of **1** could be introduced by acid-catalyzed *N*-hemiacetalization of **3** with amide **123**. The macrolactone ring could be constructed using HWE reaction and macrolactonization as critical reactions. As shown in Scheme 27, the synthesis of the C9–C20 fragment commenced from ring opening of PMB protected (*R*)-glycidol with vinyl lithium **126** (prepared from the corresponding stannane<sup>67</sup> and  $BuLi$ ). The subsequent product was protected as its pivalate ether and converted to enal **128** by a two-step procedure. Allylsilane **129** was prepared from aldehyde **92** through the three-step sequence of dibromomethylenation, Kumada–Tamao–Corriu coupling with  $TMSCH_2MgCl$ , and protodesilylation. The Hosomi–Sakurai reaction of **128** with **129** promoted by  $SnCl_4$  afforded the desired **131** (15S) in 47% yield as well as its isomer **130** (15R) in 42%

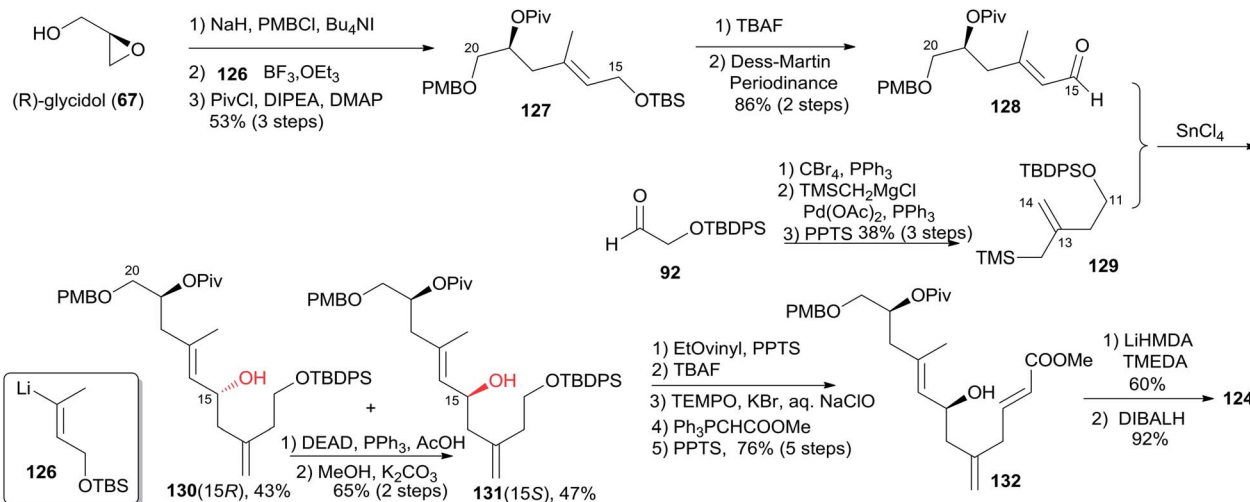


Scheme 25 Porco's synthesis of the macrolactone core of (–)-zampanolide.



Scheme 26 Uenishi's retrosynthetic analysis of (–)-zampanolide.

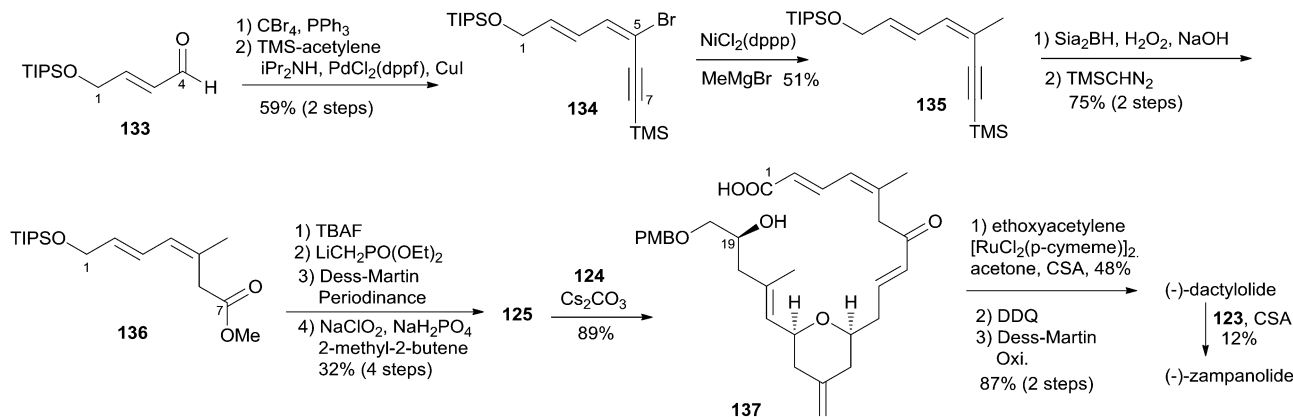




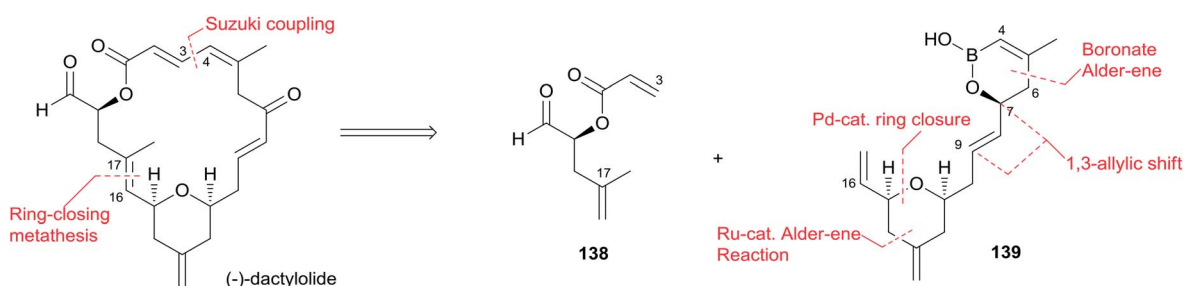
Scheme 27 Uenishi's synthesis of fragment C9–C20 of (–)-zampanolide.

yield; the latter could be converted to **131** in 65% yield by Mitsunobu reaction followed by methanolysis. Transformation of **131** to **132** proceeded through an efficient five-step sequence in 76% overall yield. The THP ring in **124** was built by intramolecular *O*-Michael reaction; the subsequent ester was reduced with DIBALH, with concomitant removal of the pivaloate group, to provide the C9–C20 fragment (**124**). The preparation of the C1–C8 fragment (**125**) started with

dibromomethylenation of aldehyde **133** followed by stereo-selective Sonogashira coupling with TMS-acetylene (Scheme 28). Introduction of a methyl group to alkyne **134** via the Kumada–Tamao–Corriu coupling proceeded with the anticipated inversion of olefin geometry.<sup>68</sup> Transformation of the terminal TMS-acetylene to ester **136** proceeded through a two-step sequence. Another four-step sequence including TIPS ether removal, diethyl methylphosphonate introduction, and



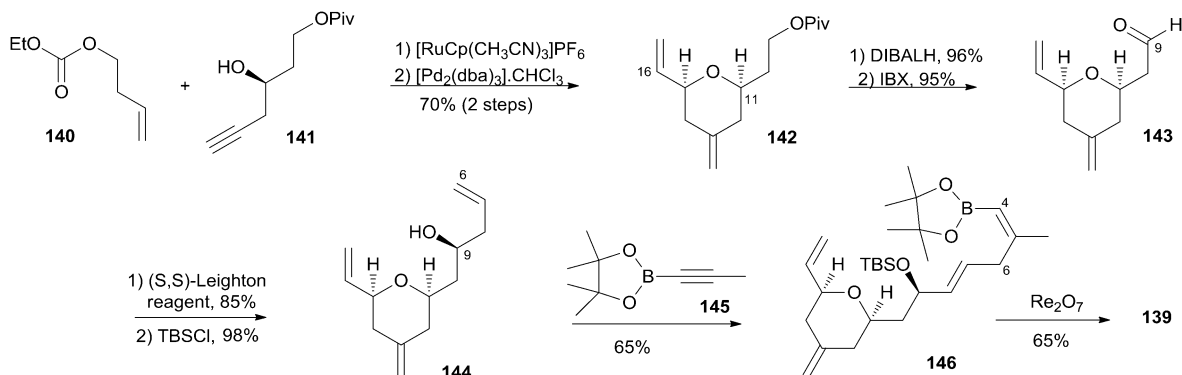
Scheme 28 Uenishi's total synthesis of (–)-zampanolide.



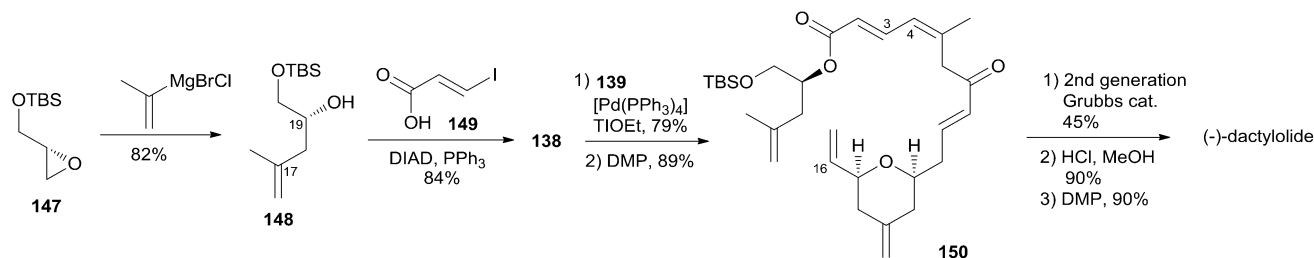
Scheme 29 Lee's retrosynthetic analysis of (–)-dactylolide.



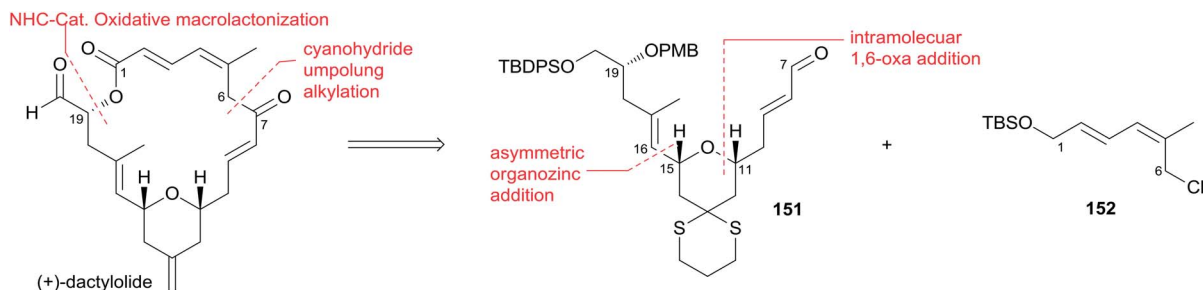




Scheme 30 Lee's synthesis of fragment C4–C16 of (–)-dactylolide.



Scheme 31 Lee's total synthesis of (–)-dactylolide.



Scheme 32 Hong's retrosynthetic analysis of (+)-dactylolide.

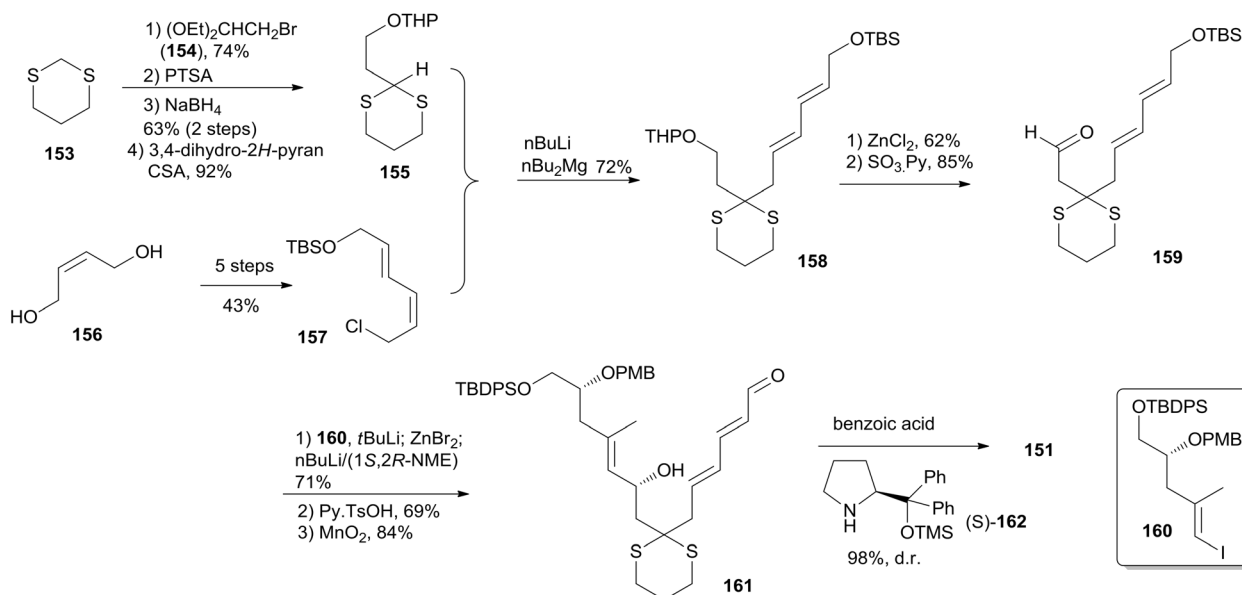
oxidations completed the synthesis of **125**. The syntheses of **3** and **1** were completed as shown in Scheme 28. The HWE reaction of aldehyde **124** and  $\beta$ -ketophosphonate **125** provided seco acid **137**, which was subjected to cyclization using the Trost–Kita method to generate a macrolactone. Dactylolide (**3**) was readily prepared from the macrolactone *via* a two-step sequence. Treatment of **3** with hexadienoylamide **123** catalyzed by CSA afforded **1** in 12% yield.

### 5.10 Lee's synthesis of (–)-dactylolide

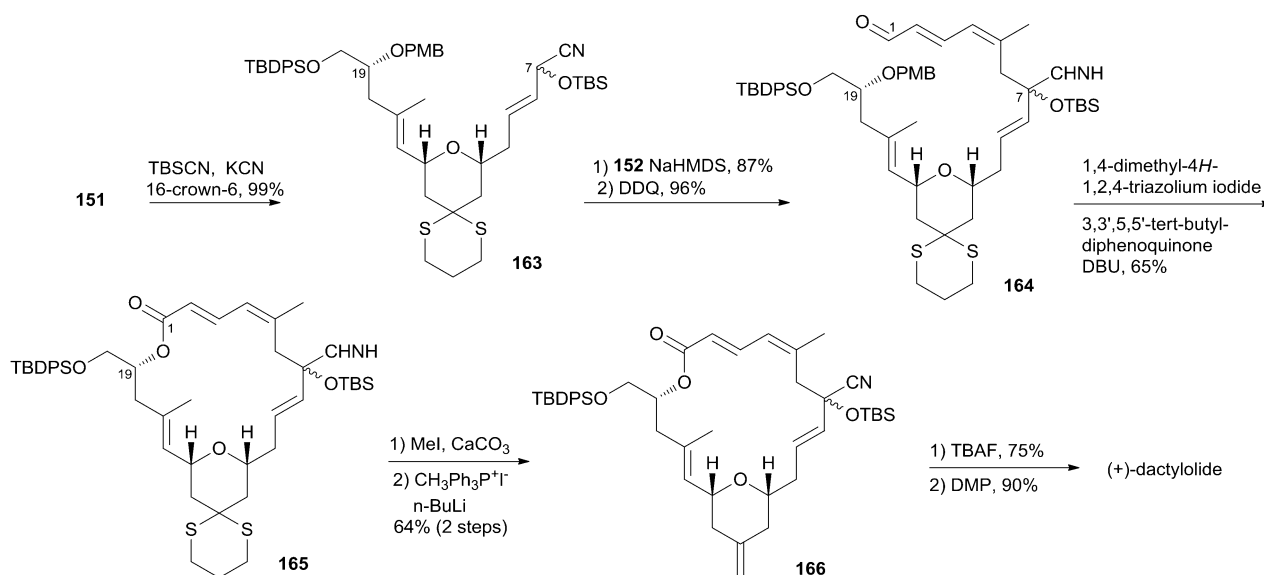
Lee's retrosynthetic analysis, as shown in Scheme 29, features the construction of C–C and C–O bonds by transition-metal-catalyzed reactions in the hope of minimizing the need for functional group transformations and protection–deprotection steps.<sup>69,70</sup> They envisioned closing the macrolactone ring through a late-stage RCM reaction at C16–C17. The C3–C4 bond

was planned to be synthesized through a Suzuki–Miyaura coupling of iodoacylate **138** and a cyclic boronic acid half ester **139**. This could be accessed through the ruthenium-catalyzed Alder–ene reaction (RCAER)<sup>71</sup> and allylic [1,3]-transposition.<sup>72</sup> The pyran subunit in **139** would be installed using a tandem RCAER and palladium-catalyzed ring closure. The synthesis of the C4–C16 fragment **139** commenced with the RCAER between ethyl carbonate **140** and homopropargylic alcohol **141** (Scheme 30).<sup>73</sup> The product was treated with palladium catalyst in the presence of Trost's chiral (+)-DPPBA ligand to afford 2,6-*cis*-disubstituted THP **142**, which was readily converted to aldehyde **143** through a deprotection–oxidation sequence. Leighton allylation followed by TBS protection afforded homoallyl silyl ether **144**. The RCAER of alkynyl boronate **145** occurred selectively with the least hindered double bond at C7 of **144**, and afforded vinyl boronate **146**. Cyclic boronic acid half ester **139** was obtained by the 1,3-transposition of the allyl alcohol of **146** with





Scheme 33 Hong's synthesis of fragment C7–C20 of (+)-dactylolide.



Scheme 34 Hong's total synthesis of (+)-dactylolide.

rhenum oxide.<sup>74</sup> 2-Iodoacrylate **138**, the Suzuki coupling partner, was prepared from TBS-protected (*S*)-glycidol **147** through the sequence shown in Scheme 31. Ester **138** was synthesized by ring opening with 2-propenylmagnesium chloride followed by Mitsunobu reaction of **148** with 2-iodoacrylic acid **149**. Suzuki coupling between **138** and **139** followed by a four-step sequence delivered (–)-dactylolide.

### 5.11 Hong's total synthesis of (+)-dactylolide

(+)-Dactylolide (**4**) was synthesized by the Hong group from 1,3-dithiane, featuring the 1,6-oxa conjugate addition reaction of a 2,4-dienal for the facile synthesis of the 2,6-*cis*-THP subunit, the

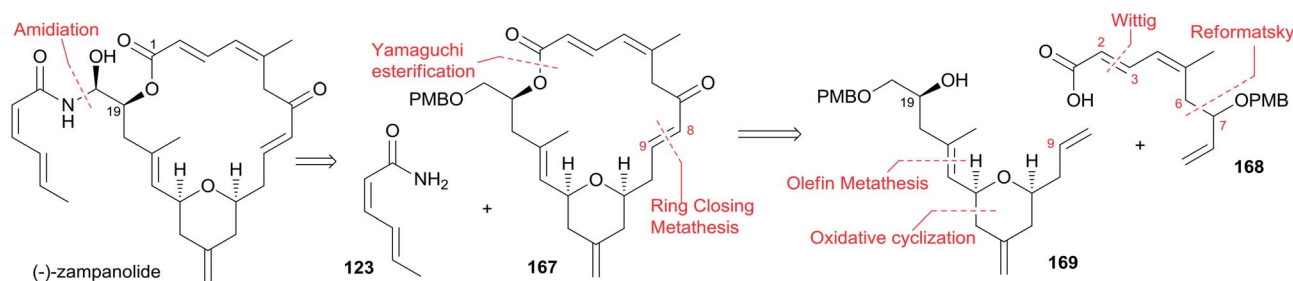
umpolung alkylation reaction of a cyanohydrin, and the *N*-heterocyclic carbene (NHC)-catalyzed oxidative macrolactonization reaction.<sup>75</sup> Hong's retrosynthetic plan for **4** is outlined in Scheme 32. The macrolactone core could be constructed from the C1–C6 fragment (**152**) and the C7–C20 fragment (**151**) by intramolecular oxidative macrolactonization of  $\omega$ -hydroxy aldehyde catalyzed by an NHC and umpolung alkylation of cyanohydrin. The synthesis of the C7–C20 fragment is shown in Scheme 33. The coupling of the dithiane **155**, prepared from dithiane **153**,<sup>76</sup> with dienyl chloride **157** (ref. 77) mediated by *n*BuLi–*n*Bu<sub>2</sub>Mg provided **158**, which was converted to aldehyde **159** through a deprotection–oxidation sequence. Stereoselective installation of the C15 secondary carbinol by an

asymmetric organozinc addition, avoiding the possible chelation of the oxygen atoms to zinc, required slow addition of **159** to a mixture of the corresponding bromozinc reagent of **160** and lithiated (1*S*, 2*R*)-NME. This procedure provided **161** in good stereoselectivity (*dr* = 7.7 : 1), and this was subjected to organocatalytic 1,6-oxa conjugate addition reaction catalyzed by (*S*)-**162** to provide the desired 2,6-*cis*-THP **151** with excellent stereoselectivity and yield, representing the first successful example of THP construction through an intramolecular 1,6-oxa conjugate addition reaction. Hong and co-workers proceeded to install the C1–C6 fragment using an acyl anion equivalent (Scheme 34). The TBS-protected cyanohydrin **163**, prepared from **151**, was coupled with dienyl chloride **152** followed by concomitant PMB removal and oxidation at C1 to generate  $\omega$ -hydroxy aldehyde **164**. NHC-catalyzed oxidative macrolactonization of **164** provided macrolactone **165**. This represents the first example of NHC-catalyzed oxidative macrolactonization of a  $\omega$ -hydroxy aldehyde. The synthesis of **4** was completed by elaborating the C13 exo-methylene group, unveiling the C7 carbonyl group, and oxidizing the C20 hydroxyl group.

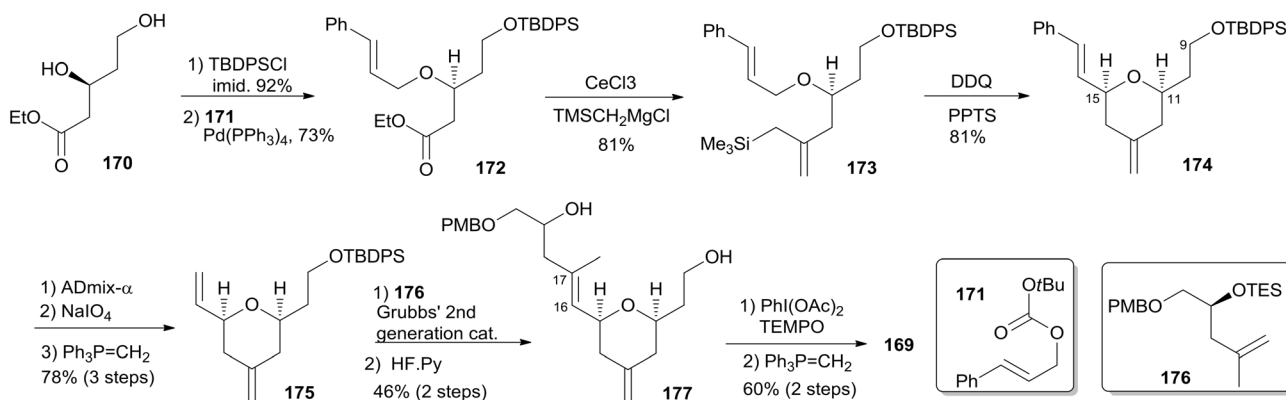
### 5.12 Ghosh's synthesis of (–)-zampanolide<sup>16,24</sup>

The Ghosh group accomplished an enantioselective total synthesis of **1** using a novel DDQ/Bronsted acid promoted cyclization as the key reaction.<sup>78</sup> Their retrosynthetic analysis is shown in Scheme 35.<sup>16,24</sup> The strategic bond disconnection of the side chain at C20 provides macrolactone **167**, which can be

constructed from the C9–C20 fragment **169** and the C1–C8 fragment **168** by Yamaguchi esterification followed by RCM. A similar RCM strategy was first employed by Hoye.<sup>18</sup> The double bond at C16–C17 in the C9–C20 fragment **169** could be installed by a cross metathesis reaction, and the THP ring could be constructed by an oxidative cyclization reaction. Fragment C1–C8 (**168**) could be built by Reformatsky reaction followed by Wittig olefination. As shown in Scheme 36, the synthesis commenced with known ester **170**.<sup>79</sup> Selective protection followed by esterification with *tert*-butyl cinnamyl carbonate (**171**) catalyzed by Pd(PPh<sub>3</sub>)<sub>4</sub> afforded cinnamyl ether **172**, which was converted to allylsilane **173** employing the procedure modified by Narayanan and Bunnelle.<sup>80</sup> Oxidative cyclization of **173** with DDQ catalyzed by PPTS constructed the 4-methylene-THP ring in **174** stereoselectively and efficiently, presumably due to the Zimmerman–Traxler transition state where all substituents are equatorially oriented. Disubstituted olefin **174** was converted to monosubstituted olefin **175** via a three-step sequence. Olefin **176** was obtained by opening PMB-protected glycidol with isopropenylmagnesium bromide followed by alcohol protection as TES ether. Grubbs cross-metathesis of **175** with **176** provided an *E/Z* olefin mixture (1.7 : 1). Removal of all silyl groups followed by chromatographic purification provided trisubstituted olefin **177**. Selective oxidation followed by Wittig olefination generated **169**. The synthesis of the C1–C8 fragment (Scheme 37) began with the preparation of allyl bromide **178**,<sup>81</sup> which was subjected to Reformatsky reaction with acrolein to give unsaturated  $\delta$ -lactone **179**. DIBAL-H reduction followed by Wittig reaction

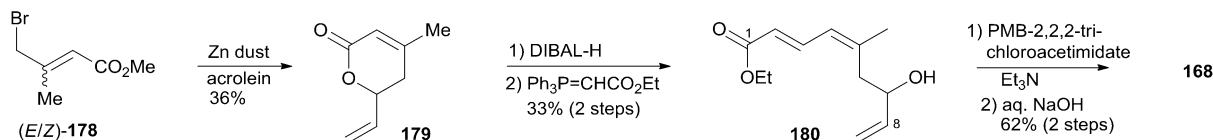


Scheme 35 Ghosh's retrosynthetic analysis of (–)-zampanolide.

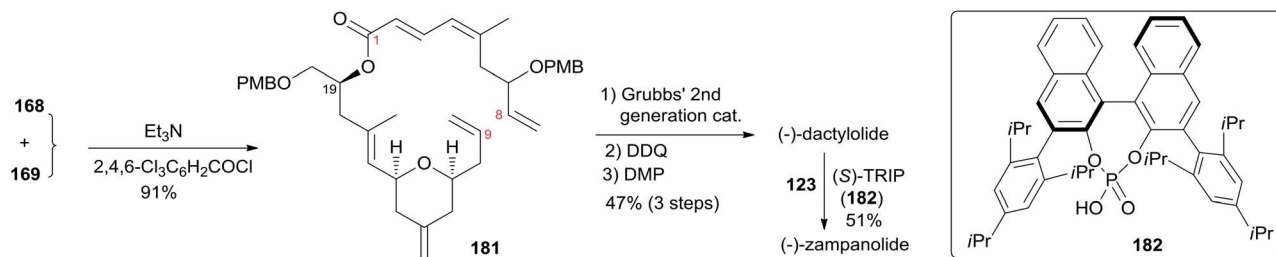


Scheme 36 Ghosh's synthesis of fragment C9–C20 of (–)-zampanolide.

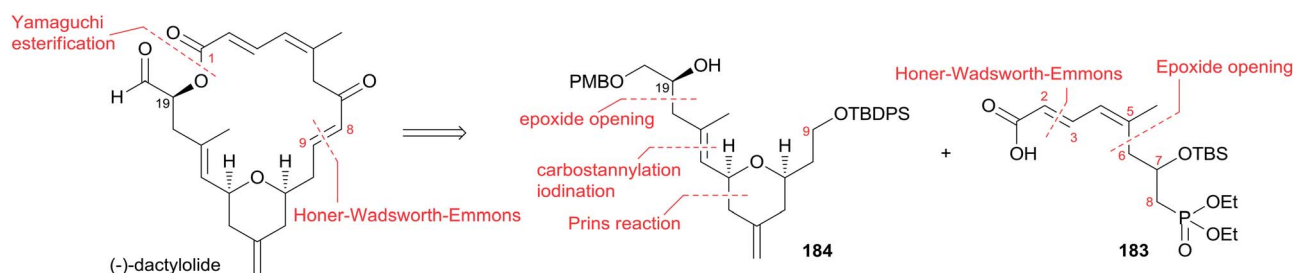




Scheme 37 Ghosh's synthesis of fragment C1–C8 of (–)-zampanolide.



Scheme 38 Ghosh's total synthesis of (–)-zampanolide.

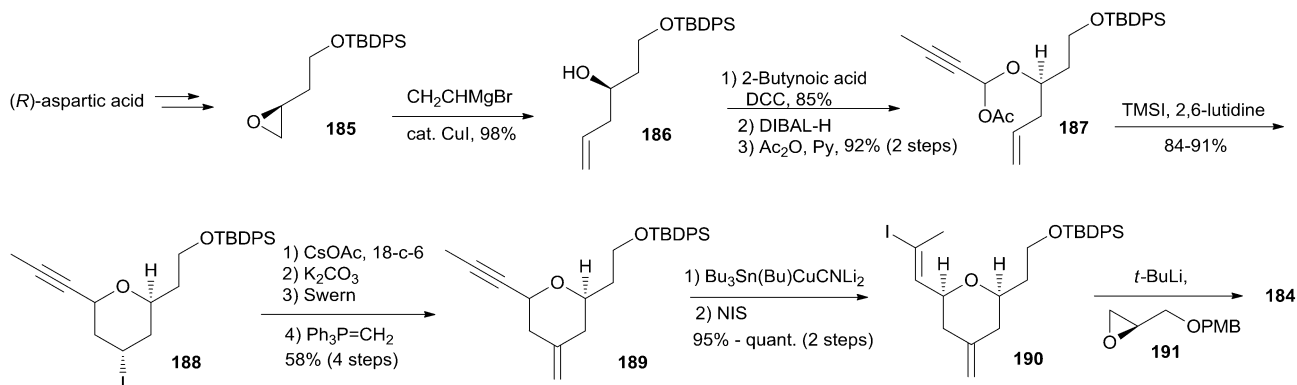


Scheme 39 Altmann's retrosynthetic analysis of (–)-dactylolide.

afforded allylic alcohol **180**. Fragment C1–C8 (**168**) was prepared from **180** through a protection-saponification sequence. The completion of the synthesis (Scheme 38) started with Yamaguchi esterification of acid **168** with alcohol **169** to furnish **181**, which was subjected to Grubbs RCM reaction. The subsequent macrolactone was converted to **3** by a deprotection–oxidation sequence. The conversion of **3** to **1** was completed by treatment of aldehyde **3** with amide **123** in the presence of (*S*)-TRIP (**182**) in 51% yield.

### 5.13 Altmann's total synthesis of (–)-zampanolide<sup>17,82</sup>

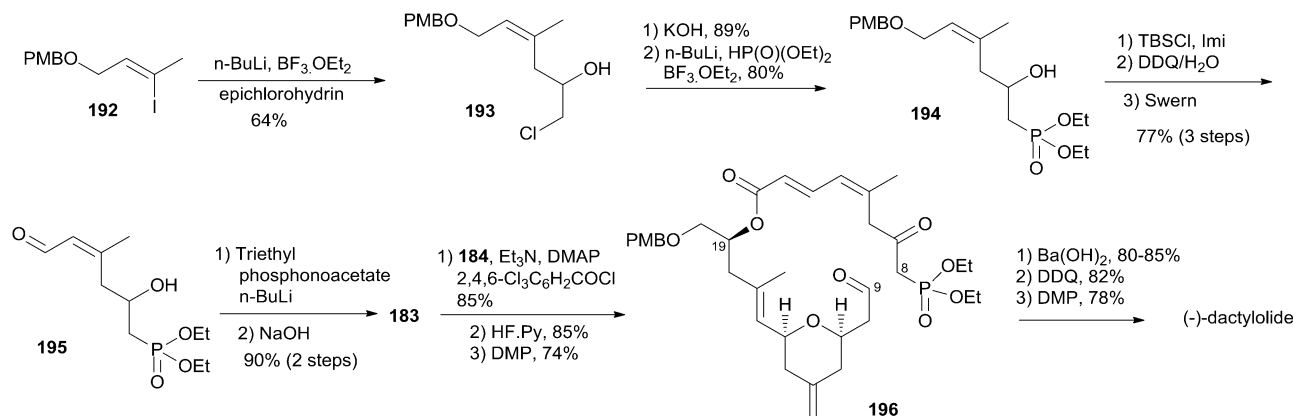
Altmann's retrosynthetic analysis for **3** (Scheme 39) is centred on HWE macrocyclization involving the formation of the C8–C9 double bond.<sup>17,82</sup> The requisite precursor would be obtained *via* ester formation between the C1–C8 fragment (**183**) and the C9–C20 fragment (**184**). The synthesis of the C9–C20 fragment **184** started with the Cu-mediated regioselective epoxide opening of **185**, prepared from (*R*)-aspartic acid in three steps, with vinyl-MgBr (Scheme 40). Alcohol **186** was then elaborated into THP



Scheme 40 Altmann's synthesis of fragment C9–C20 of (–)-dactylolide.







Scheme 41 Altmann's total synthesis of (–)-dactylolide.

**188** in a highly stereoselective Prins-type reaction employing a segment coupling approach as developed by Rychnovsky.<sup>83</sup> In a first step, this involved esterification of **186** with 2-butyric acid, which was followed by DIBAL-H reduction of the ester and trapping of the aluminated intermediate at  $-78^{\circ}\text{C}$  with  $\text{Ac}_2\text{O}$  to furnish **187**. Treatment of **187** with TMSI gave substituted THP **188** with the desired 2,6-*syn* relationship and the iodine located *anti* to the substituents in the 2- and 6-positions. This is in line with previous observations by Rychnovsky for related transformations. Conversion of **188** to **189** was achieved by a four-step sequence: iodide displacement with  $\text{CsOAc}/18\text{-crown-6}$ , hydrolysis, Swern oxidation, and Wittig reaction. Conversion of **189** to the desired *E*-vinyl iodide **190** was achieved with  $\text{Bu}_3\text{Sn}(\text{Bu})\text{CuCNLi}_2$  generated *in situ* followed by  $\text{Sn-I}$  exchange with NIS. Reaction of vinyl iodide **190** with PMB-protected (*R*)-glycidol **191** generated fragment C9–C20 (**184**). Unsaturated acid **183** was prepared by coupling of lithiated *Z*-vinyl iodide **192** (obtained in two steps from 2-butyne-1-ol) and epichlorohydrin mediated by  $\text{BF}_3\cdot\text{OEt}_2$  (Scheme 41). Treatment of **193** with base followed by  $\text{BF}_3$ -mediated epoxide opening with lithiated diethylphosphite gave  $\beta$ -hydroxyphosphonate **194**, which was converted to aldehyde **195** through a protection–deprotection–oxidation sequence. HWE reaction followed by basic hydrolysis then afforded the desired acid **183**. The final assembly of (–)-dactylolide commenced with esterification of alcohol **184** with acid **183** (Scheme 41) under Yamaguchi conditions to give an ester which was converted to HWE precursor **196** through a global desilylation–oxidation sequence. Ring-closure step was achieved with  $\text{Ba}(\text{OH})_2$  as an optimized base and the synthesis of **3** was completed by PMB removal and DMP oxidation.

Conversion of **3** to **1** was brought about by Hoyer's aza-aldol reaction with (*Z,E*)-sorbamide,<sup>18</sup> which gave a mixture of **1** and *epi-1* in 18% and 12% yield respectively.

#### 5.14 Summary and evaluation

The common feature for all syntheses is to begin with construction of the macrolactone core and to end with installation of the *N*-acyl hemiaminal side chain. The longest linear steps together with the overall yields for these total syntheses are listed in Table 5. The Hoyer and Uenishi routes are the most

convergent and efficient of the dactylolide syntheses, and the Porco partial synthesis is also efficient, although it has yet to be elaborated to dactylolide. The approaches by Altmann and Jennings are strategically attractive due to their efficiency, even though they have longer linear sequences.

The Achilles' heel of the approaches to zampanolide is the stereospecific construction of the *N*-acylhemiaminal group, and this was a challenging step in all the synthetic routes to this compound. Smith and co-workers constructed the *N*-acyl hemiaminal in their synthesis of **2** using a stereospecific Curtius rearrangement as a key step.<sup>12</sup> Hoyer and co-workers used an aluminium aza-aldol addition reaction to construct the *N*-acyl hemiaminal, but did not report their yield. C20 epimerization is a key issue for these two methods. The conversion of **3** to **1** was completed in Uenishi's synthesis in only 12% yield. To improve this reaction, Ghosh and co-workers investigated *N*-acyl aminal formation between aldehyde **3** and amide **123** in the presence of matched chiral phosphoric acid (*S*)-TRIP (**182**, 20 mol%). These

Table 5 Summary of total syntheses

Compound	Approach	Linear steps	Overall yield	Ref.
(+)-Zampanolide	Smith	28	0.25%	10 and 13
(–)-Zampanolide	Altmann	22	0.9%	17 and 82
(–)-Zampanolide	Ghosh	20	0.9%	16 and 24
(–)-Zampanolide	Uenishi	18	0.6%	11
(–)-Zampanolide	Hoyer	14 <sup>a</sup>	— <sup>b</sup>	18
(–)-Dactylolide	Hoyer	17 <sup>a</sup>	1.3%	18
(–)-Dactylolide	Hoyer	13 <sup>a</sup>	21%	18
(–)-Dactylolide	Jennings	25	4.3%	19
(–)-Dactylolide	McLeod	16 <sup>a</sup>	2.5%	20
(–)-Dactylolide	Uenishi	17	5.2%	11
(–)-Dactylolide	Lee	20	2.4%	69
(+)-Dactylolide	Hong	20	1.5%	75
(–)-Dactylolide	Ghosh	19	1.8%	16 and 24
(–)-Dactylolide	Altmann	21	5.2%	17 and 82
(+)-Dactylolide	Floreancig	20	2.1%	21
(+)-Dactylolide	Keck	24	3.6%	15
Macrolactone	Porco	13	4.5%	58

<sup>a</sup> The approach used a known fragment; the linear steps and overall yield were counted from the known fragment as a starting material.

<sup>b</sup> The yield for the last step was not reported.



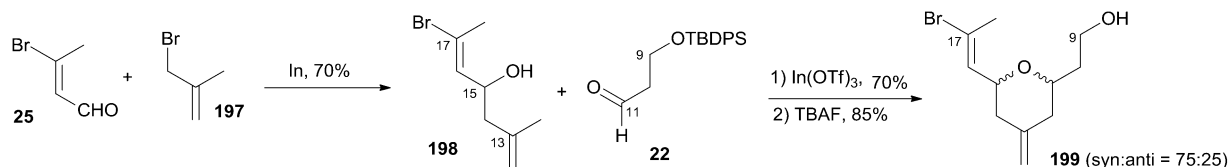
reaction conditions furnished **1** in 51% yield, so at this point this is the most attractive and efficient approach.<sup>16,24</sup>

The general strategies to close macrolactone rings are the Yamaguchi esterification, the Horner–Emmons macrocyclization, and ring-closing metathesis. Three additional methods were developed for this reaction: NHC-catalyzed oxidative macrolactonization (Hong),<sup>75</sup> macrocyclization of a vinylstannane (Porco),<sup>58</sup> and macrolactonization *via* Ti(IV) mediated ring-opening of an epoxide (Hoye).<sup>18</sup> The macrolactone contains three chiral centres at C11, C15, and C19. The C19 chiral centre was generally obtained from the chiral pool (*e.g.* (*S*)-glycidol). The reported syntheses focus on diastereoselective construction of the 2,6-*cis*-disubstituted THP subunit containing the C11 and C15 chiral centres and on the efficient construction of the macrolactone core.

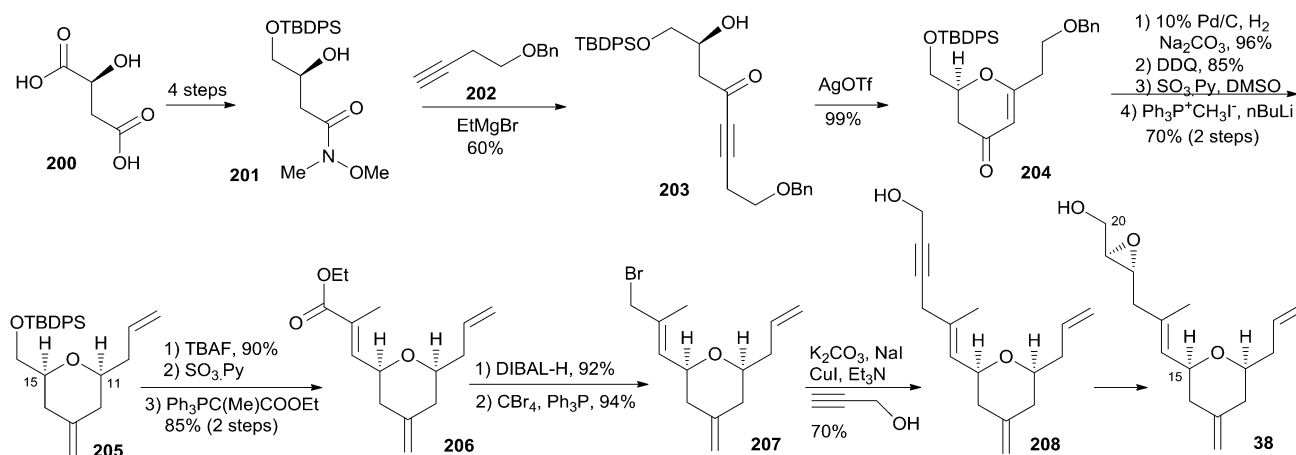
## 6. Other synthetic studies

### 6.1 Construction of *cis* 2,6-disubstituted THP rings

As shown in Scheme 42, Loh and co-workers reported a diastereoselective construction of fragment C9–C17 of zampanolide *via* In(OTf)<sub>3</sub>-catalyzed intramolecular 2,5-oxonium-ene cyclization from enal **25**.<sup>84</sup> In(OTf)<sub>3</sub>-catalyzed intramolecular 2,5-oxonium-ene cyclization of **198** and aldehyde **22**, followed by desilylation with TBAF, provided the desired cyclization product **199** with good *syn* diastereoselectivity (75 : 25) as two inseparable isomers. The observed predominant 2,6-*syn* selectivity can be rationalized by the cyclic six-membered chair-like transition state favouring an all-equatorial substitution pattern.



Scheme 42 Loh's synthesis of fragment C9–C17 of zampanolide.

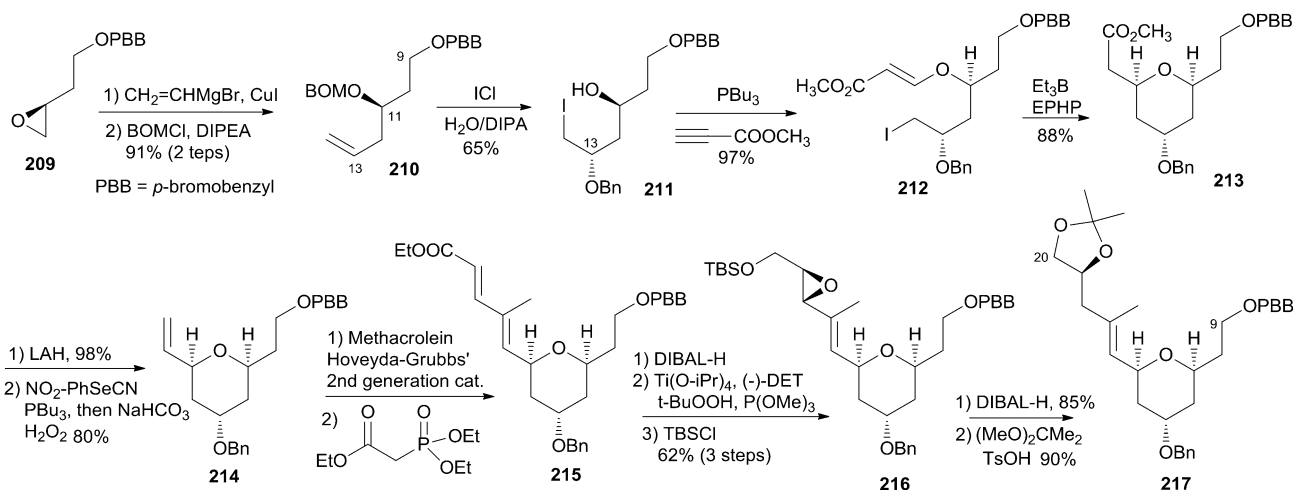


Scheme 43 Reddy's synthesis of fragment C8–C20 of (–)-zampanolide.

Reddy and co-workers reported a new synthetic route for the known pyran-containing subunit **38** (ref. 85) that had been synthesized by Hoye and co-workers.<sup>18</sup> The synthesis began with the known Weinreb amide **201** (Scheme 43), which was obtained in four steps from L-malic acid following a reported protocol.<sup>86</sup> The initial four-carbon extension was achieved by the addition of homopropargyl benzyl ether (**202**) to Weinreb amide **201**, which gave the desired alkynone **203**. Key cyclization of the alkynone gave pyranone **204**. THP **205** was obtained from **204** *via* sequential reduction, DDQ benzyl removal, oxidation, and Wittig olefination. Conversion of **205** to ester **206** was achieved by a deprotection–oxidation–Wittig reaction sequence. Bromide **207** was achieved by reduction of ester **206** and subsequent treatment with CBr<sub>4</sub> and PPh<sub>3</sub>. A three-carbon unit was introduced to compound **207** through a CuI/K<sub>2</sub>CO<sub>3</sub>/NaI-mediated coupling reaction to give **208**. Reduction of the alkyne to the desired *trans*-olefin followed by Sharpless asymmetric epoxidation gave target compound **38**.

Taylor and co-workers applied their recently developed methodology<sup>87</sup> to assemble the 4-alkoxy-2,6-*cis*-THP **217** from an advanced sulfonyl pyran fragment. The synthesis commenced with preparation of **210** as illustrated in Scheme 44. The epoxide **209** was prepared from (*R*)-aspartic acid *via* modification of the literature's procedure.<sup>88</sup> Regioselective epoxide opening with vinyl magnesium bromide in the presence of catalytic CuI followed by *p*-bromobenzyloxy methyl ether alkylation gave the PBB ether **210**. Electrophilic activation of the resulting ether with ICl at low temperature provided exclusively 1,3-*syn* diol monoether. PPh<sub>3</sub>-catalyzed conjugate addition of alcohol **211** to methyl propiolate yielded β-alkoxyacrylate **212**. Intramolecular





Scheme 44 Taylor's synthesis of fragment C9–C20 of (–)-zampanolide.

radical cyclization promoted by  $\text{Et}_3\text{B}$  in the presence of 1-ethylpiperidinium hypophosphate gave THP **213** in good diastereoselectivity ( $>20:1$ ). Reduction followed by Grieco–Sharpless olefination provided **214**. Exposure of terminal olefin **214** to excess methacrolein mediated by Hoveyda–Grubbs' second-generation catalyst followed by HWE olefination gave dienonate **215**. Reduction of the dienonate with DIBAL-H followed by Sharpless epoxidation and *in situ* silyl protecting gave alcohol **216**. Completion of the C9–C20 fragment was accomplished *via* regioselective opening of the vinyl epoxide with DIBAL-H at low temperature. Desilylation followed by acetone formation provided **217**.

## 6.2 Preparation of *N*-acyl hemiaminal model systems

Porco and Troast reported<sup>59</sup> the synthesis of *N*-acyl hemiaminal model systems related to the side chain of zampanolide. Key steps involve oxidative decarboxylation of *N*-acyl- $\alpha$ -amino acid intermediates, followed by ytterbium triflate mediated solvolysis. This method has not yet been applied to the installation of the hemiaminal side chain of zampanolide.

## 7. Conclusions

Zampanolide has been demonstrated as a very promising MSA with potent cytotoxicity against both drug sensitive and multi-drug resistant cancer cell lines. It can promote tubulin assembly in a paclitaxel-like manner. Its mechanism of action has been shown to involve covalent binding to  $\beta$ -tubulin at residues Asn<sup>228</sup> and His<sup>229</sup> at the taxane luminal site, and the use of its side chain to induce structuring of the M-loop into a short helix. Despite isolation from two marine organisms and several total syntheses, samples of zampanolide remain scarce. Moreover, only a few analogs have been reported to date. Future work on this promising compound needs to include both more efficient and practical approaches to the synthesis of (–)-zampanolide to provide larger quantities for in-depth investigation of its

cytotoxic activity, and the design and construction of novel (–)-zampanolide analogues to further investigate the SAR of this very promising class of natural products.

## Acknowledgements

California State University (CSU), Fresno and the NIH RIMI program at CSU Fresno (P20MD002732) are acknowledged for partial support of this work.

## References

- 1 S. B. Horwitz, *J. Nat. Prod.*, 2004, **67**, 136–138.
- 2 P. B. Schiff, J. Fant and S. B. Horwitz, *Nature*, 1979, **277**, 665–667.
- 3 D. G. I. Kingston, *J. Nat. Prod.*, 2009, **72**, 507–515.
- 4 D. G. I. Kingston, in *Anticancer Agents from Natural Products*, eds. G. M. Cragg, D. G. I. Kingston and D. J. Newman, CRC press, Boca Raton, FL, 2nd edn, 2012, pp. 123–176.
- 5 R. M. Borzilleri and G. D. Vite, in *Ann. Rep. Med. Chem.*, 2009, vol. 44, ch. 15, pp. 301–322.
- 6 C. C. Rohena and S. L. Mooberry, *Nat. Prod. Rep.*, 2014, **31**, 335–355.
- 7 J. Tanaka and T. Higa, *Tetrahedron Lett.*, 1996, **37**, 5535–5538.
- 8 J. J. Field, A. J. Singh, A. Kanakkanthara, T. i. Halafihi, P. T. Northcote and J. H. Miller, *J. Med. Chem.*, 2009, **52**, 7328–7332.
- 9 A. Cutignano, I. Bruno, G. Bifulco, A. Casapullo, C. Debitus, L. Gomez-Paloma and R. Riccio, *Eur. J. Org. Chem.*, 2001, 775–778.
- 10 A. B. Smith, I. G. Safonov and R. M. Corbett, *J. Am. Chem. Soc.*, 2002, **124**, 11102–11113.
- 11 J. Uenishi, T. Iwamoto and J. Tanaka, *Org. Lett.*, 2009, **11**, 3262–3265.
- 12 A. B. Smith III, I. G. Safonov and R. M. Corbett, *J. Am. Chem. Soc.*, 2001, **123**, 12426–12427.
- 13 A. B. Smith III and I. G. Safonov, *Org. Lett.*, 2002, **4**, 635–637.



- 14 E. M. Larsen, M. R. Wilson, J. Zajicek and R. E. Taylor, *Org. Lett.*, 2013, **15**, 5246–5249.
- 15 C. C. Sanchez and G. E. Keck, *Org. Lett.*, 2005, **7**, 3053–3056.
- 16 A. K. Ghosh and X. Cheng, *Org. Lett.*, 2011, **13**, 4108–4111.
- 17 D. Zurwerra, F. Glaus, L. Betschart, J. Schuster, J. Gertsch, W. Ganci and K.-H. Altmann, *Chem.-Eur. J.*, 2012, **18**, 16868–16883.
- 18 T. R. Hoye and M. Hu, *J. Am. Chem. Soc.*, 2003, **125**, 9576–9577.
- 19 F. Ding and M. P. Jennings, *J. Org. Chem.*, 2008, **73**, 5965–5976.
- 20 I. Louis, N. L. Hungerford, E. J. Humphries and M. D. McLeod, *Org. Lett.*, 2006, **8**, 1117–1120.
- 21 D. L. Aubele, S. Wan and P. E. Floreancig, *Angew. Chem., Int. Ed.*, 2005, **44**, 3485–3488.
- 22 T. Higa, J. Tanaka and D. Garcia Gravalos, *International Pat.*, WO9710242 (A1) 1997.
- 23 J. J. Field, B. Pera, E. Calvo, A. Canales, D. Zurwerra, C. Trigili, J. Rodriguez-Salarichs, R. Matesanz, A. Kanakkanthara, S. J. Wakefield, A. J. Singh, J. Jimenez-Barbero, P. Northcote, J. H. Miller, J. A. Lopez, E. Hamel, I. Barasoain, K.-H. Altmann and J. F. Diaz, *Chem. Biol.*, 2012, **19**, 686–698.
- 24 A. K. Ghosh, X. Cheng, R. Bai and E. Hamel, *Eur. J. Org. Chem.*, 2012, **2012**, 4130–4139.
- 25 C. Dumontet and M. A. Jordan, *Nat. Rev. Drug Discovery*, 2010, **9**, 790–803.
- 26 J. H. Miller, A. J. Singh and P. T. Northcote, *Mar. Drugs*, 2010, **8**, 1059–1079.
- 27 E. Nogales, S. G. Wolf, I. A. Khan, R. F. Luduena and K. H. Downing, *Nature*, 1995, **375**, 424–427.
- 28 F. Diaz Jose, I. Barasoain and M. Andreu Jose, *J. Biol. Chem.*, 2003, **278**, 8407–8419.
- 29 R. M. Buey, E. Calvo, I. Barasoain, O. Pineda, M. C. Edler, R. Matesanz, G. Cerezo, C. D. Vanderwal, B. W. Day, E. J. Sorensen, J. A. Lopez, J. M. Andreu, E. Hamel and J. F. Diaz, *Nat. Chem. Biol.*, 2007, **3**, 117–125.
- 30 E. Calvo, I. Barasoain, R. Matesanz, B. Pera, E. Camafeita, O. Pineda, E. Hamel, C. D. Vanderwal, J. M. Andreu, J. A. Lopez and J. F. Diaz, *Biochemistry*, 2012, **51**, 329–341.
- 31 J. T. Huzil, J. K. Chik, G. W. Slys, H. Freedman, J. Tuszynski, R. E. Taylor, D. L. Sackett and D. C. Schriemer, *J. Mol. Biol.*, 2008, **378**, 1016–1030.
- 32 M. J. Bennett, K. Barakat, J. T. Huzil, J. Tuszynski and D. C. Schriemer, *Chem. Biol.*, 2010, **17**, 725–734.
- 33 J. J. Field, E. Calvo, P. T. Northcote, J. H. Miller, K.-H. Altmann and J. F. Diaz, *Methods Cell Biol.*, 2013, **115**, 303–325.
- 34 I. Barasoain, A. M. Garcia-Carril, R. Matesanz, G. Maccari, C. Trigili, M. Mori, J.-Z. Shi, W.-S. Fang, J. M. Andreu, M. Botta and J. F. Diaz, *Chem. Biol.*, 2010, **17**, 243–253.
- 35 R. M. Buey, I. Barasoain, E. Jackson, A. Meyer, P. Giannakakou, I. Paterson, S. Mooberry, J. M. Andreu and J. F. Diaz, *Chem. Biol.*, 2005, **12**, 1269–1279.
- 36 R. Matesanz, I. Barasoain, C.-G. Yang, L. Wang, X. Li, C. de Ines, C. Coderch, F. Gago, J. J. Barbero, J. M. Andreu, W.-S. Fang and J. F. Diaz, *Chem. Biol.*, 2008, **15**, 573–585.
- 37 M. C. Edler, R. M. Buey, R. Gussio, A. I. Marcus, C. D. Vanderwal, E. J. Sorensen, J. F. Diaz, P. Giannakakou and E. Hamel, *Biochemistry*, 2005, **44**, 11525–11538.
- 38 A. E. Protá, K. Bargsten, D. Zurwerra, J. J. Field, J. F. Diaz, K.-H. Altmann and M. O. Steinmetz, *Science*, 2013, **339**, 587–590.
- 39 E. Nogales, M. Whittaker, R. A. Milligan and K. H. Downing, *Cell*, 1999, **96**, 79–88.
- 40 F. J. Fourniol, C. V. Sindelar, B. Amigues, D. K. Clare, G. Thomas, M. Perderiset, F. Francis, A. Houdusse and C. A. Moores, *J. Cell Biol.*, 2010, **191**, 463–470.
- 41 S.-Y. Liao, G.-Q. Mo, J.-C. Chen and K.-C. Zheng, *J. Mol. Model.*, 2014, **20**, 2070.
- 42 M. Shindo, *Top. Heterocycl. Chem.*, 2006, **5**, 179–254.
- 43 E. Sharif and G. A. O'Doherty, *Chemtracts*, 2009, **22**, 67–79.
- 44 C. M. Rojas, in *Name Reactions for Homologations, Part 2*, ed. L. J. Li, Wiley, Hoboken, NJ, 2009, pp. 136–163.
- 45 M. L. Morin-Fox and M. A. Lipton, *Tetrahedron Lett.*, 1993, **34**, 7899–7902.
- 46 A. B. Smith III, R. J. Fox and T. M. Razler, *Acc. Chem. Res.*, 2008, **41**, 675–687.
- 47 M. Oizumi, M. Takahashi and K. Ogasawara, *Synlett*, 1997, 1111–1113.
- 48 P. Somfai and R. Olsson, *Tetrahedron*, 1993, **49**, 6645–6650.
- 49 L. E. Overman and L. D. Pennington, *J. Org. Chem.*, 2003, **68**, 7143–7157.
- 50 D. R. Williams, M. P. Clark and M. A. Berliner, *Tetrahedron Lett.*, 1999, **40**, 2287–2290.
- 51 D. A. Evans, E. Hu, J. D. Burch and G. Jaeschke, *J. Am. Chem. Soc.*, 2002, **124**, 5654–5655.
- 52 F. Ding and M. P. Jennings, *Org. Lett.*, 2005, **7**, 2321–2324.
- 53 G. E. Keck, J. A. Covel, T. Schiff and T. Yu, *Org. Lett.*, 2002, **4**, 1189–1192.
- 54 W. C. Still, C. Gennari, J. A. Noguez and D. A. Pearson, *J. Am. Chem. Soc.*, 1984, **106**, 260–262.
- 55 G. E. Keck, C. Sanchez and C. A. Wager, *Tetrahedron Lett.*, 2000, **41**, 8673–8676.
- 56 A. G. Dossetter, T. F. Jamison and E. N. Jacobsen, *Angew. Chem., Int. Ed.*, 1999, **38**, 2398–2400.
- 57 A. Fuerstner, O. R. Thiel, L. Ackermann, H.-J. Schanz and S. P. Nolan, *J. Org. Chem.*, 2000, **65**, 2204–2207.
- 58 D. M. Troast, J. Yuan and J. A. Porco Jr, *Adv. Synth. Catal.*, 2008, **350**, 1701–1711.
- 59 D. M. Troast and J. A. Porco Jr, *Org. Lett.*, 2002, **4**, 991–994.
- 60 B. Leroy and I. E. Marko, *Tetrahedron Lett.*, 2001, **42**, 8685–8688.
- 61 S. Kiyooka, K. Suzuki, M. Shirouchi, Y. Kaneko and S. Tanimori, *Tetrahedron Lett.*, 1993, **34**, 5729–5732.
- 62 J. M. Bobbitt, *J. Org. Chem.*, 1998, **63**, 9367–9374.
- 63 S. Takano, T. Kamikubo, T. Sugihara, M. Suzuki and K. Ogasawara, *Tetrahedron: Asymmetry*, 1993, **4**, 201–204.
- 64 T. Hanazawa, K. Sasaki, Y. Takayama and F. Sato, *J. Org. Chem.*, 2003, **68**, 4980–4983.
- 65 B. M. Trost, S. A. King and T. Schmidt, *J. Am. Chem. Soc.*, 1989, **111**, 5902–5915.
- 66 H. Oda, T. Kobayashi, M. Kosugi and T. Migita, *Tetrahedron*, 1995, **51**, 695–702.



- 67 J. Uenishi, R. Kawahama, O. Yonemitsu, A. Wada and M. Ito, *Angew. Chem., Int. Ed.*, 1998, **37**, 320–323.
- 68 J. Uenishi, K. Matsui and M. Ohmi, *Tetrahedron Lett.*, 2005, **46**, 225–228.
- 69 Y. Yun Sang, C. Hansen Eric, I. Volchkov, J. Cho Eun, Y. Lo Wai and D. Lee, *Angew. Chem., Int. Ed.*, 2010, **49**, 4261–4263.
- 70 D. Lee and I. Volchkov, *Strategies Tactics Org. Synth.*, 2012, **8**, 171–197.
- 71 B. M. Trost, M. U. Frederiksen and M. T. Rudd, *Angew. Chem., Int. Ed.*, 2005, **44**, 6630–6666.
- 72 S. Bellemin-Laponnaz, H. Gisie, J. P. Le Ny and J. A. Osborn, *Angew. Chem., Int. Ed. Engl.*, 1997, **36**, 976–978.
- 73 G. Pattenden, M. A. Gonzalez, P. B. Little, D. S. Millan, A. T. Plowright, J. A. Tornos and T. Ye, *Org. Biomol. Chem.*, 2003, **1**, 4173–4208.
- 74 E. C. Hansen and D. Lee, *J. Am. Chem. Soc.*, 2006, **128**, 8142–8143.
- 75 K. Lee, H. Kim and J. Hong, *Angew. Chem., Int. Ed.*, 2012, **51**, 5735–5738.
- 76 M. J. Gaunt, A. S. Jessiman, P. Orsini, H. R. Tanner, D. F. Hook and S. V. Ley, *Org. Lett.*, 2003, **5**, 4819–4822.
- 77 F. Caussanel, P. Deslongchamps and Y. L. Dory, *Org. Lett.*, 2003, **5**, 4799–4802.
- 78 Y. Hayashi and T. Mukaiyama, *Chem. Lett.*, 1987, 1811–1814.
- 79 M. M. Claffey, C. J. Hayes and C. H. Heathcock, *J. Org. Chem.*, 1999, **64**, 8267–8274.
- 80 B. A. Narayanan and W. H. Bunnelle, *Tetrahedron Lett.*, 1987, **28**, 6261–6264.
- 81 B. Lei and A. G. Fallis, *Can. J. Chem.*, 1991, **69**, 1450–1456.
- 82 D. Zurwerra, J. Gertsch and K.-H. Altmann, *Org. Lett.*, 2010, **12**, 2302–2305.
- 83 S. D. Rychnovsky, Y. Hu and B. Ellsworth, *Tetrahedron Lett.*, 1998, **39**, 7271–7274.
- 84 T.-P. Loh, J.-Y. Yang, L.-C. Feng and Y. Zhou, *Tetrahedron Lett.*, 2002, **43**, 7193–7196.
- 85 C. R. Reddy and B. Srikanth, *Synlett*, 2010, 1536–1538.
- 86 T. Shioiri, N. McFarlane and Y. Hamada, *Heterocycles*, 1998, **47**, 73–76.
- 87 M. R. Wilson and R. E. Taylor, *Org. Lett.*, 2012, **14**, 3408–3411.
- 88 J. A. Frick, J. B. Klassen, A. Bathe, J. M. Abramson and H. Rapoport, *Synthesis*, 1992, 621–623.

